ARMY RESEARCH LABORATORY

Investigation of Failed Components from a 7-in High Altitude Research Program (HARP) Cannon

by Scott M. Grendahl, Matthew Motyka, and Sean Fudger

NOTICES

Disclaimers

Army Research Laboratory

Aberdeen Proving Ground, MD 21005-5059

Investigation of Failed Components from a 7-in High Altitude Research Program (HARP) Cannon

Scott M. Grendahl
Weapons and Materials Research Directorate, ARL

Matthew Motyka
Data Matrix Solutions Inc.

Sean Fudger
Oak Ridge Institute for Science and Education

REPORT DOCUMENTATION PAGE		*Form Approved* *OMB No. 0704-0188*

1. REPORT DATE *(DD-MM-YYYY)*	2. REPORT TYPE	3. DATES COVERED *(From - To)*
November 2011	Final	September 2010–December 2010

4. TITLE AND SUBTITLE	5a. CONTRACT NUMBER
Investigation of Failed Components from a 7-in High Altitude Research Program (HARP) Cannon	
	5b. GRANT NUMBER
	5c. PROGRAM ELEMENT NUMBER

6. AUTHOR(S)	5d. PROJECT NUMBER
Scott M. Grendahl, Matthew Motyka,[*] and Sean Fudger[†]	622618H80
	5e. TASK NUMBER
	5f. WORK UNIT NUMBER

7. PERFORMING ORGANIZATION NAME(S) AND ADDRESS(ES)	8. PERFORMING ORGANIZATION REPORT NUMBER
U.S. Army Research Laboratory ATTN: RDRL-WMM-F Aberdeen Proving Ground, MD 21005-5059	ARL-TR-5814

9. SPONSORING/MONITORING AGENCY NAME(S) AND ADDRESS(ES)	10. SPONSOR/MONITOR'S ACRONYM(S)
	11. SPONSOR/MONITOR'S REPORT NUMBER(S)

12. DISTRIBUTION/AVAILABILITY STATEMENT

Approved for public release; distribution is unlimited.

13. SUPPLEMENTARY NOTES

[*]Data Matrix Solutions Inc., Herndon, VA, 21071
[†]Oak Ridge Institute for Science and Education, Oak Ridge, TN, 37831

14. ABSTRACT

The U.S. Army Research Laboratory (ARL) experienced a failure during a test firing of a 7-in High Altitude Research Program (HARP) cannon at EF-9 on 13 October 2010. Subsequently, a team was formed and an investigation into the mishap was conducted. The Lightweight and Specialty Metals Branch (LSMB) within the Materials and Manufacturing Sciences Division (MMSD) was tasked with conducting a failure investigation of two components determined to have catastrophically failed during the initial event. The HARP firing system is comprised of two M113A1 cannon tubes spliced together and frequently mounted on M174 recoil units. In this work, an M113A1 cannon breech assembly spindle (associated with tube 7719 and extension tube 7093) and an M174 recoil unit replenisher/recuperator tube were evaluated. Additional components of the complete assembly failed and/or experienced cracking during the event, such as the breech carrier and primer lock; however, the failures of these components were considered secondary and not the focus of this investigation.

15. SUBJECT TERMS

HARP, barrel, failure analysis

16. SECURITY CLASSIFICATION OF:			17. LIMITATION OF ABSTRACT	18. NUMBER OF PAGES	19a. NAME OF RESPONSIBLE PERSON Scott M. Grendahl
a. REPORT	b. ABSTRACT	c. THIS PAGE	UU	52	19b. TELEPHONE NUMBER *(Include area code)*
Unclassified	Unclassified	Unclassified			410-306-0819

Contents

List of Figures

List of Tables

1. Background

The U.S. Army Research Laboratory (ARL) experienced a failure during a test firing of a 7-in High Altitude Research Program (HARP) cannon at EF-9 on 13 October 2010. Subsequently, a team was formed and an investigation into the mishap was conducted. The Lightweight and Specialty Metals Branch (LSMB) within the Materials and Manufacturing Sciences Division (MMSD) was tasked with conducting a failure investigation of two components determined to have catastrophically failed during the initial event. The HARP firing system is comprised of two M113A1 cannon tubes spliced together, frequently mounted on M174 recoil units. In this work, an M113A1 cannon breech assembly spindle (associated with tube 7719 and extension tube 7093) and an M174 recoil unit replenisher/recuperator tube were evaluated. Additional components of the complete assembly failed and/or experienced cracking during the event, such as the breech carrier and primer lock; however, these components were considered secondary and not the focus of this investigation.

The investigation was conducted in a twofold manner: first, we examined the recoil unit tube and then the breech spindle. These components are shown in their as-received condition in figures 1 and 2.

Figure 1. As-received M113A1 breech assembly spindle.

Figure 2. As-received M174 recoil unit replenisher/recuperator tube.

2. M174 Recoil Unit Replenisher/Recuperator Tube Examination

2.1 Visual and Light Optical Microscopy

The external surfaces of the M174 recoil unit tube were photographed and examined for defects and/or witness marks from impact, installation, or corrosion. This component was removed from the M174 recoil unit by removing the locking nut on the fixed end of the tube. The other end was visibly bent (figure 2) and the joint failed at the nut-stud/coupling interface as observed during the initial inspection after the event. The locking nut remained on its respective coupling with the ferrule after the failure. Since there were no visible metal fracture surfaces, the failed joint design and surfaces were examined. There were no observable impact marks on the tube, which would have caused the tube to become dislodged from its mount. The nut and ferrule removed from the failed end of the tube are shown in figures 3 and 4.

Considerable care was taken to match up the ferrule with its original location on the tube. Witness marks were identified and mated with corresponding marks on the interior of the ferrule. This was done in an attempt to ensure that the joint was properly installed as designed. Figures 5 and 6 present "side A" of the ferrule and the failed end of the tube in their approximate original position as determined from the witness marks observed. Measurements of these locations can be observed in figure 6. Figures 7 and 8 present "side B" of the ferrule and the failed end of the tube in their approximate original position as determined from the witness marks observed. The corresponding measurements are available in figure 8.

2
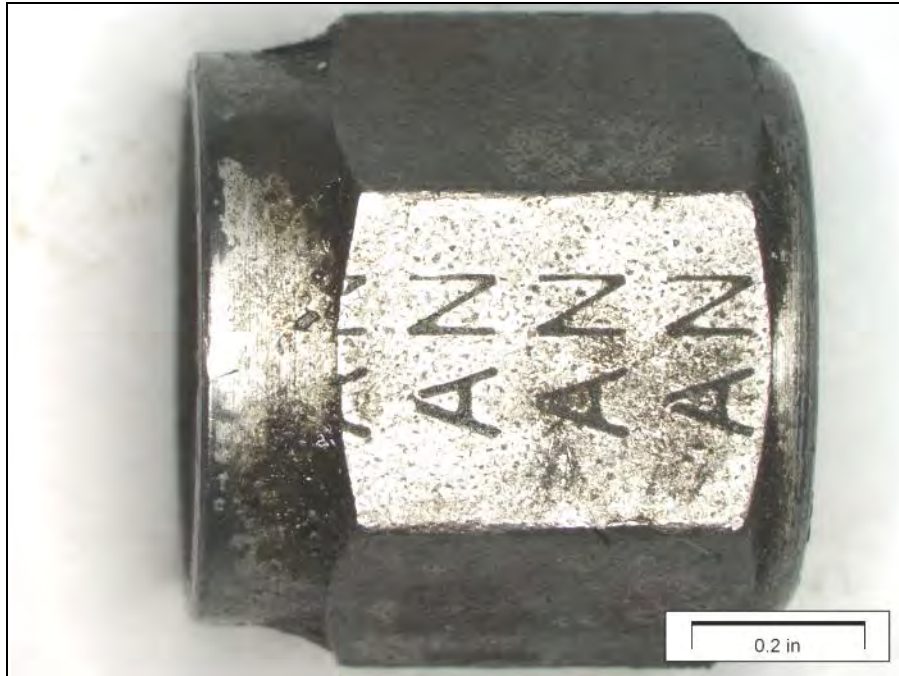
Figure 3. Nut from the failed end of the tube.
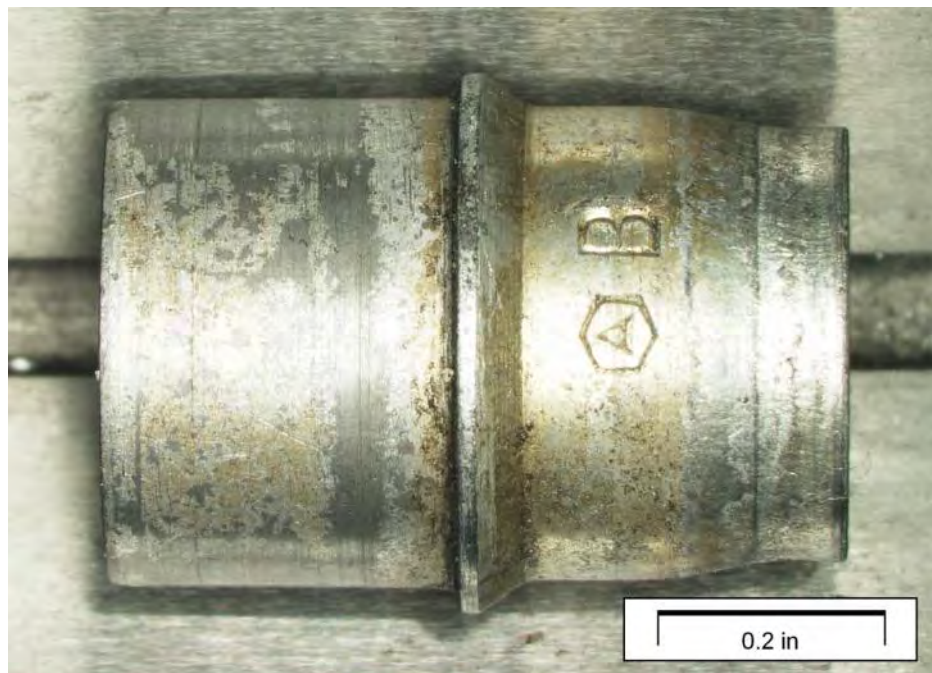
Figure 4. Ferrule from the failed end of the tube.

Figure 5. Ferrule position matched with the failed end of the tube, side A.

Figure 6. Measurements of ferrule position matched with the failed end of the tube, side A.
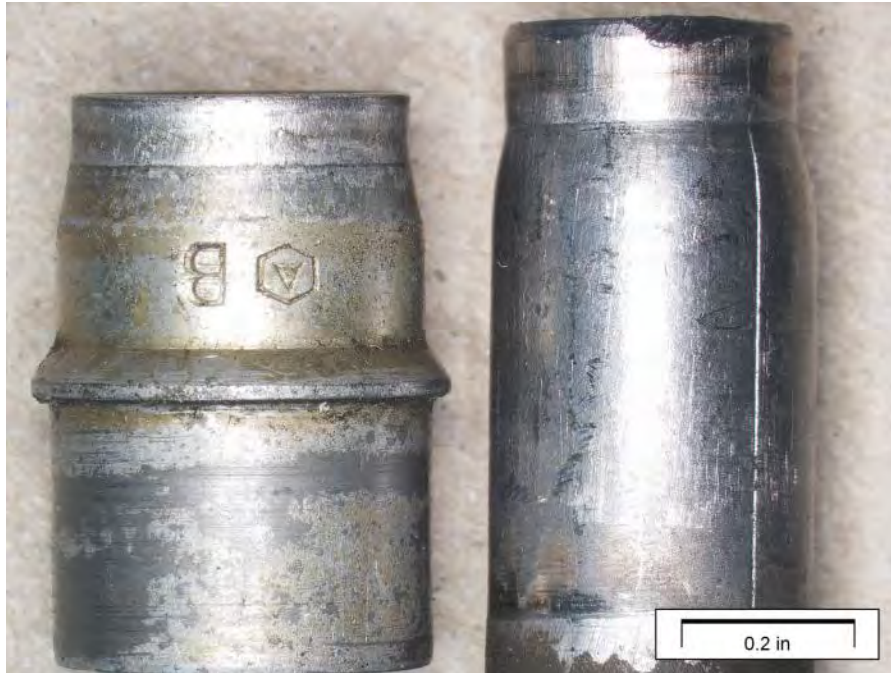
Figure 7. Ferrule position matched with the failed end of the tube, side B.

Figure 8. Measurements of ferrule position matched with the failed end of the tube, side B.

The joint on the failed end was then compared with the dissembled intact end of the tube. This comparison would provide insight on the original joint design and the intended dimensions. Figures 9–12 show both sides of the intact end of the tube as well as a dimensional analysis of these areas.
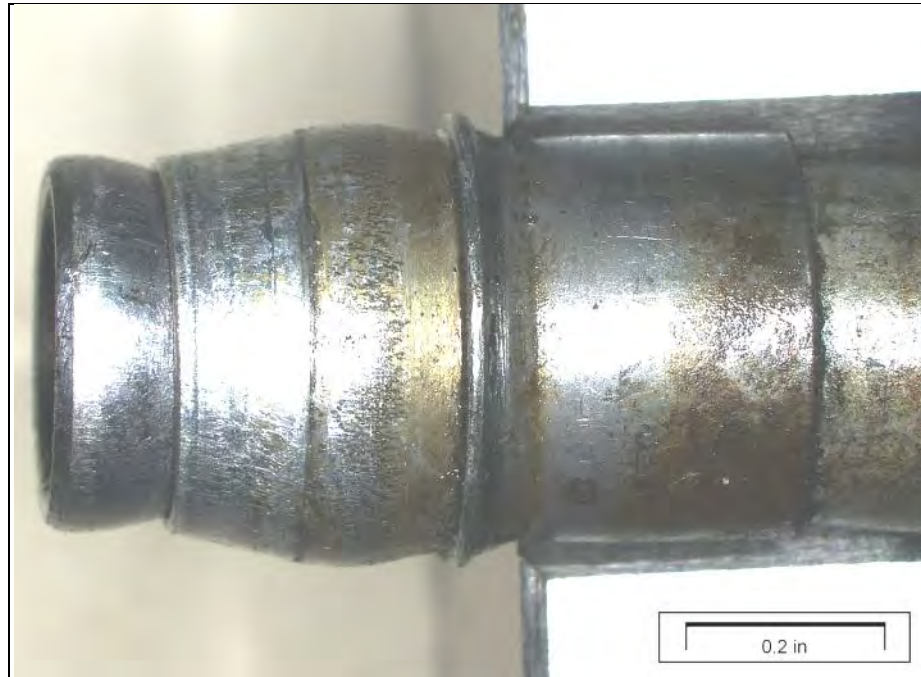
Figure 9. Intact end of the tube, side A.
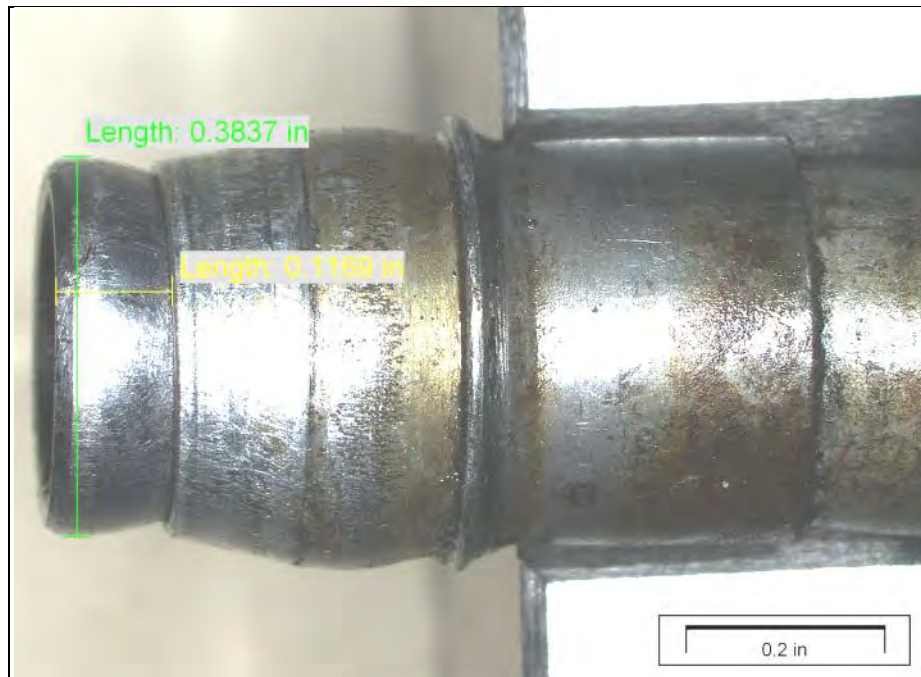
Figure 10. Intact end of the tube with measurements, side A.
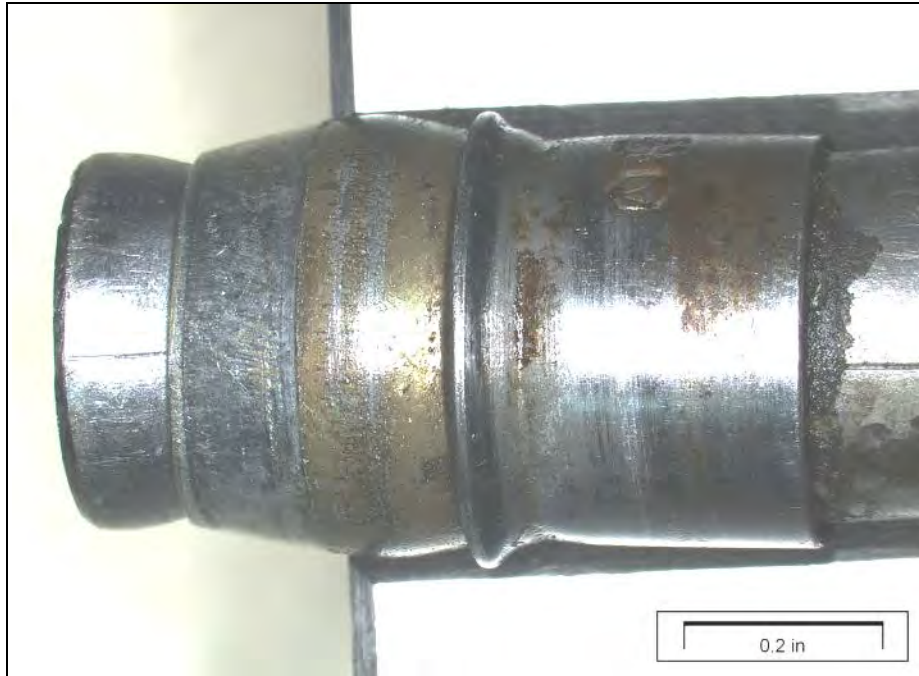
Figure 11. Intact end of the tube, side B.

Figure 12. Intact end of the tube with measurements, side B.

7

This analysis demonstrated several things. The resting place of the ferrule on the failed end of the tube was considerably closer to the end of the tube when compared with the intact end. The tubing was also visibly flared on each end. The flare on the failed end was less than on the intact end; however, this would have likely been affected by the forcing of the tube out of the ferrule. The ferrule from the intact end was carefully sectioned from the tube without damaging the underlying surfaces. Both sides of the intact end of the tube can be observed after the removal of the ferrule in figures 13−16, with and without dimensional measurements.
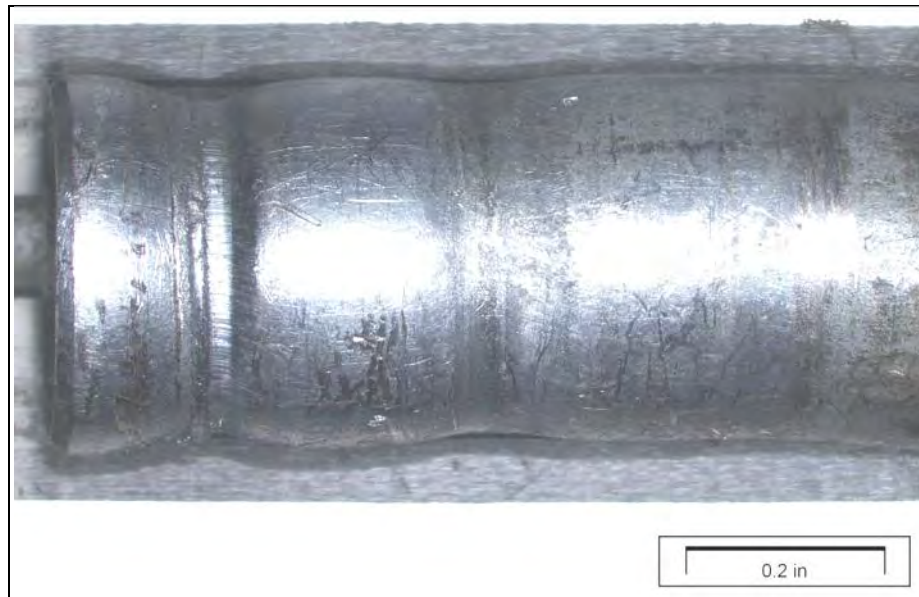
Figure 13. Intact end of the tube with ferrule removed, side A.
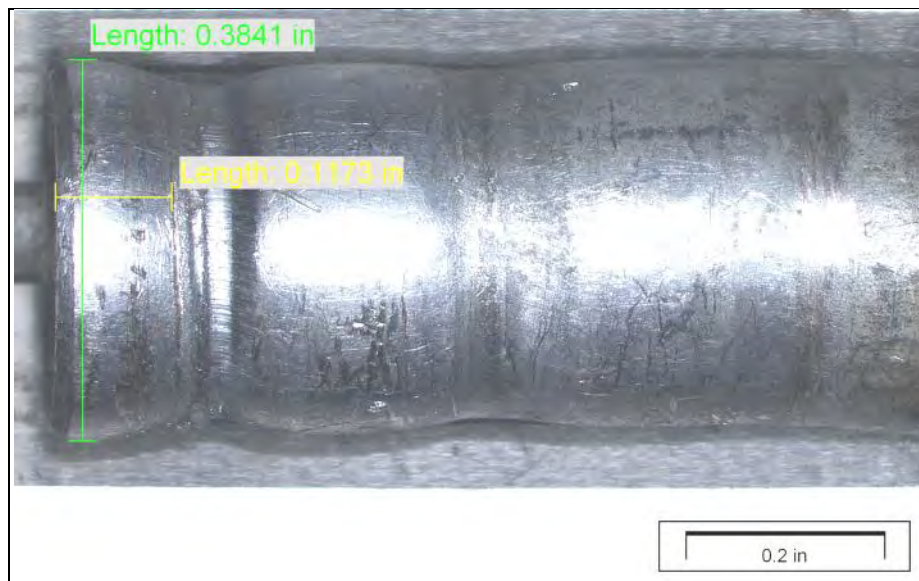
Figure 14. Measurements from intact end of the tube with ferrule removed, side A.

8
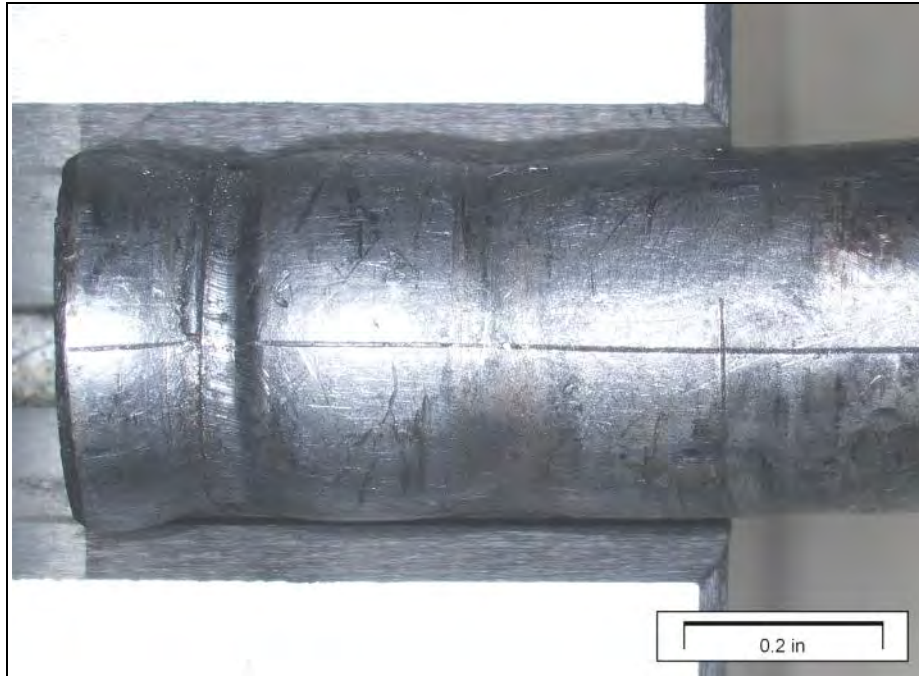
Figure 15. Intact end of the tube with ferrule removed, side B.
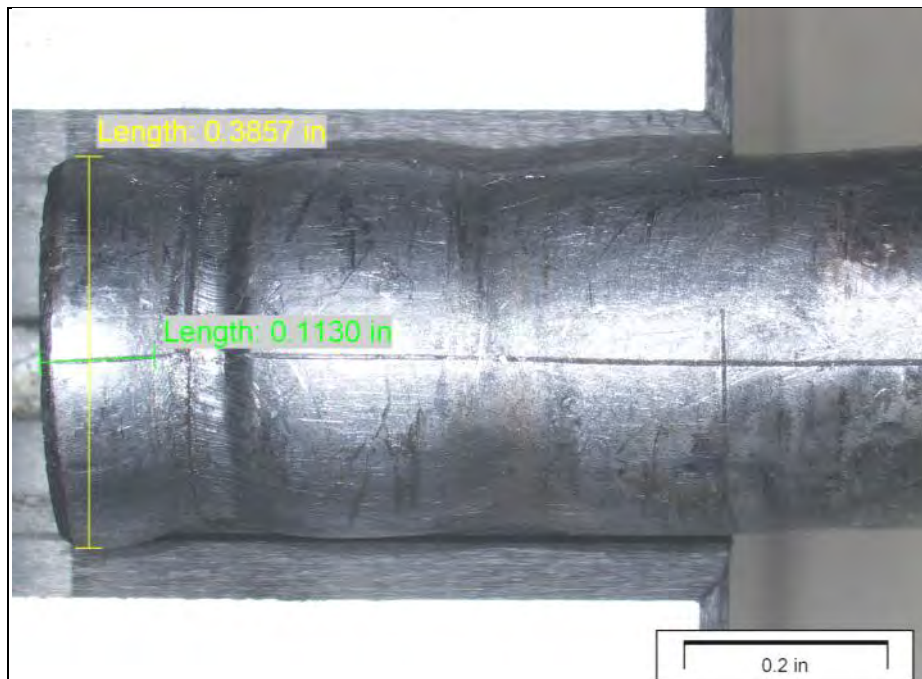
Figure 16. Measurements from intact end of the tube with ferrule removed, side B.

The M174 hydraulic line joints examined have an interesting design. Hydraulic joints are usually either a compression or flare type. In compression joints, the ferrule is compressed between the nut and the end fitting causing it to clamp down on the tubing by a reduction in the inner diameter (ID) of the ferrule. The ends of the tubing are not usually flared. In flare joints, the tubing ends are flared and the tubing is sandwiched between the end fitting and the ferrule, or between the end fitting and the nut itself, if the design doesn't include a ferrule. In either case, the tubing is physically sandwiched and held in place by the torque of the nut. Both joint designs are shown by example in figures 17 and 18. The flare design is a much more secure fitting and will hold a much greater line pressure than a simple compression fitting. The actual design in this case appeared to have traits of both types. The tubing was flared before installation; however, the tubing was not sandwiched between clamped metal surfaces. It was most similar to a normal compression design type. A schematic of the actual design used on the M174 recoil unit can be observed in figure 19 and compared with both figures 17 and 18.
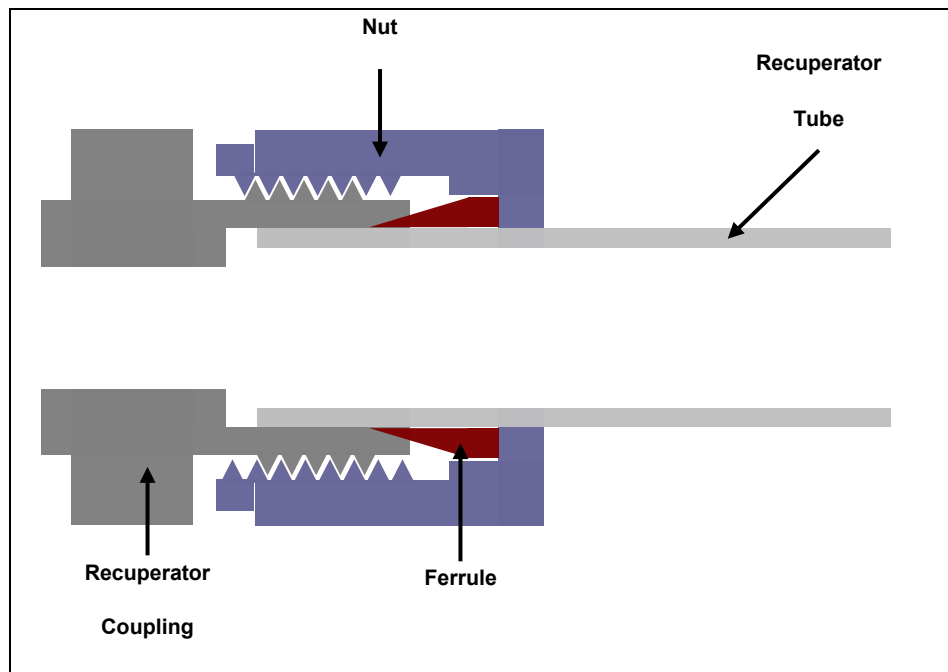
Figure 17. Typical compression fitting design.
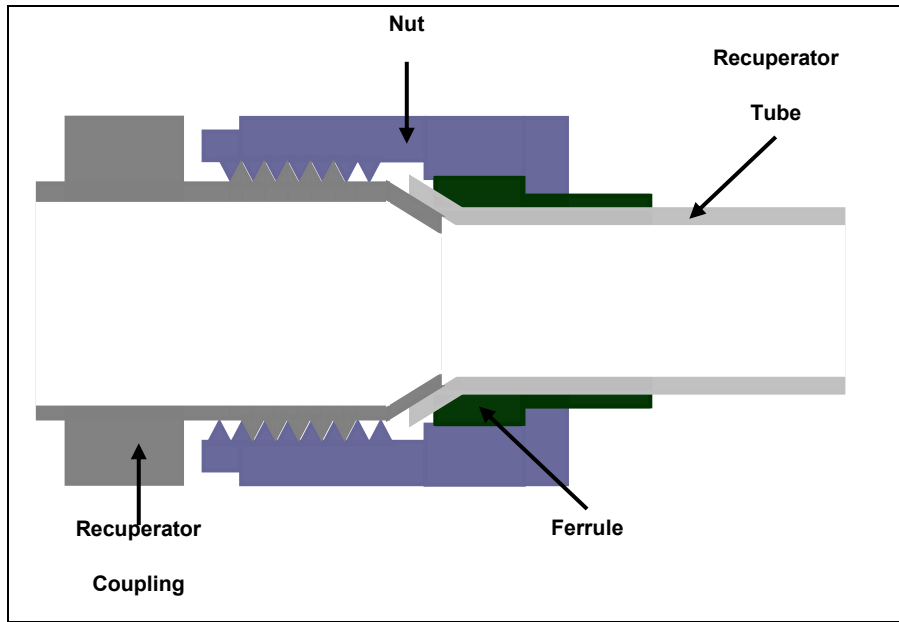
Figure 18. Typical flare fitting design.
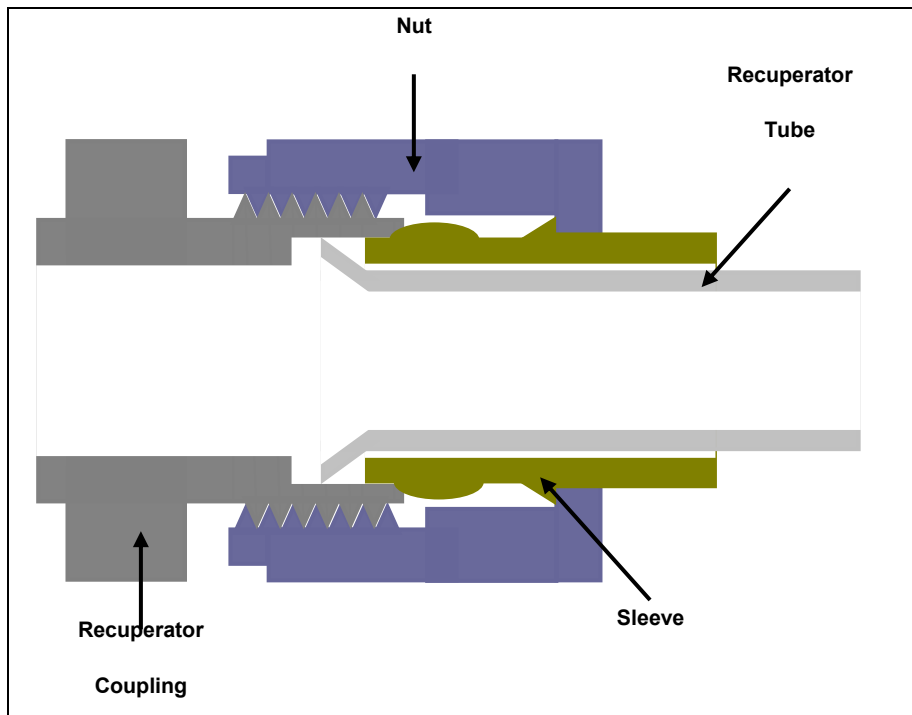
Figure 19. Schematic of the hydraulic line joints on the M174 recoil unit.

2.2   Energy Dispersive Spectroscopy (EDS)

The chemistry of the failed tube was determined with EDS and compared with that of known materials frequently used in the tubing industry. The elemental composition conformed to that of ASTM-A-254 (1) spiral-wound copper-brazed steel. Figure 20 presents the EDS spectrum obtained from the M174 recoil unit failed tube. Table 1 shows the elemental composition in comparison to known accepted values for ASTM-A 254 (1) steel. It should be noted that performing EDS analysis to determine carbon and sulfur levels is extremely inaccurate. EDS is a very useful tool for analyzing metallic and semi-metallic elements of higher atomic number. Experience using this tool and analyzing the resultant data confirms that the material in this case was ASTM-A-254 (*1*) steel. A cross section of the material can be observed in section 2.4.
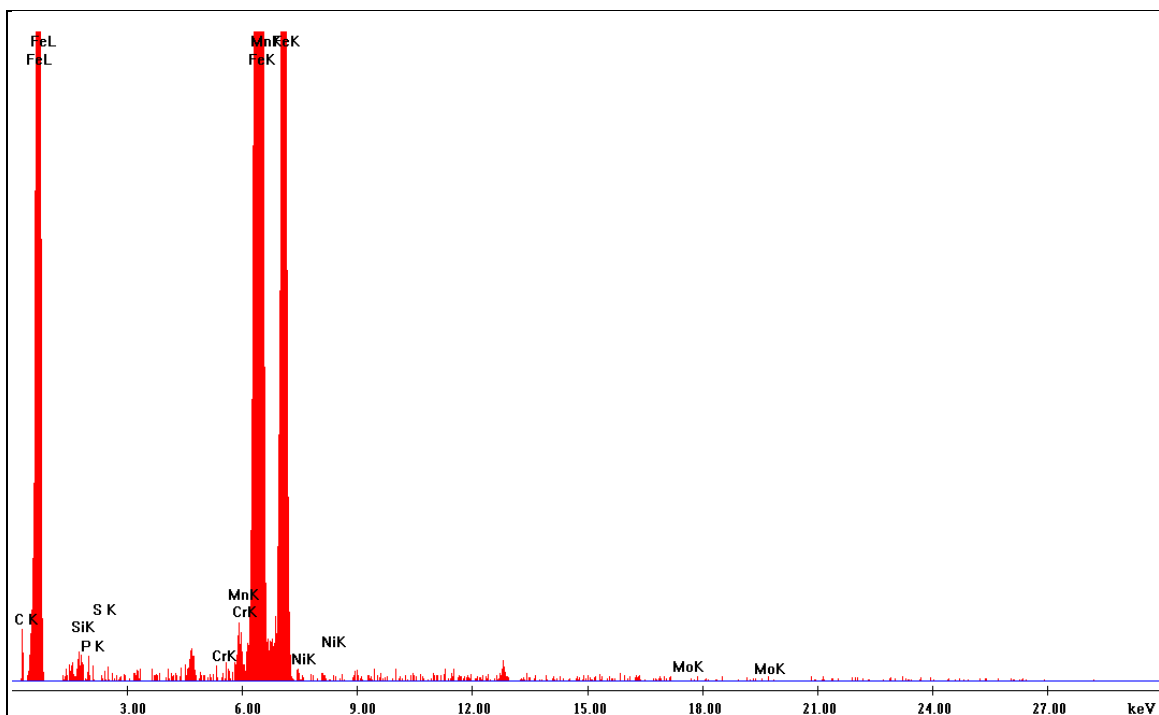
Figure 20. EDS spectrum from the failed M174 recoil unit tube.

Table 1. Elemental composition of the M174 recoil unit tube.

Element	Run No. 1 Weight-Percent	Run No. 2 Weight-Percent	Run No. 3 Weight-Percent	Run No. 4 Weight-Percent	ASTM-A-254 (1) Values Weight-Percent
Carbon	1.75	2.57	2.86	2.58	0.05–0.15
Silicon	0.23	0.17	0.10	0.19	0.00
Phosphorus	0.03	0.00	0.00	0.00	0.035 (max)
Sulfur	0.02	0.07	0.04	0.04	0.035 (max)
Chromium	0.01	0.04	0.08	0.03	0.00
Manganese	0.42	0.55	0.42	0.44	0.27–0.63
Iron	97.14	96.41	95.96	96.67	Balance
Nickel	0.10	0.09	0.12	0.06	0.00
Molybdenum	0.29	0.09	0.43	0.00	0.00
Total	**100**	**100**	**100**	**100**	**100**

2.3   Hardness

The hardness of the material was measured with Rockwell Hardness Vickers indentation on a cross-sectional mount in Bakelite, since the component was a round tube. These values were then converted to Rockwell Hardness on the "B" scale, in accordance with ASTM-E-140 (2). Table 2 presents the hardness data for the M174 recoil unit tube. The hardness conforms to that expected from the material, ASTM-A-254 (1) steel.

Table 2. Hardness data for the M174 recoil unit tube.

Reading Number	Vickers Hardness	Rockwell B Hardness
1	116	66
2	109	62
3	103	58
4	103	58
5	105	59
Average	**107.2**	**60.7**
Standard Deviation	**5.5**	

2.4   Metallography

The microstructure of the M174 recoil unit tube was analyzed by polishing and nital etching a cross-sectional mount obtained from a radial cut of the tube. Figure 21 shows the cross section. The single-strip type of spiral-wound and copper-brazed steel tube can be observed on this figure as well as the overall cross-sectional dimensions. The polished and etched microstructure can be observed in figure 22. The structure consists of primarily ferrite and is consistent with that expected for this alloy.
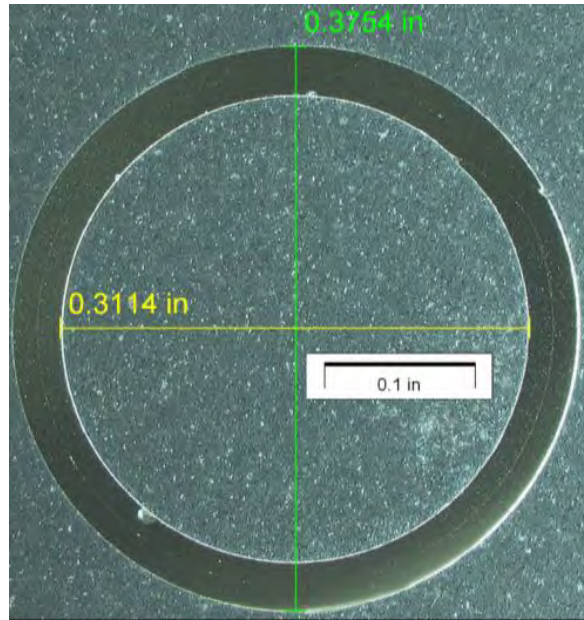
Figure 21. Cross section of the failed M174 recoil
unit tube material.
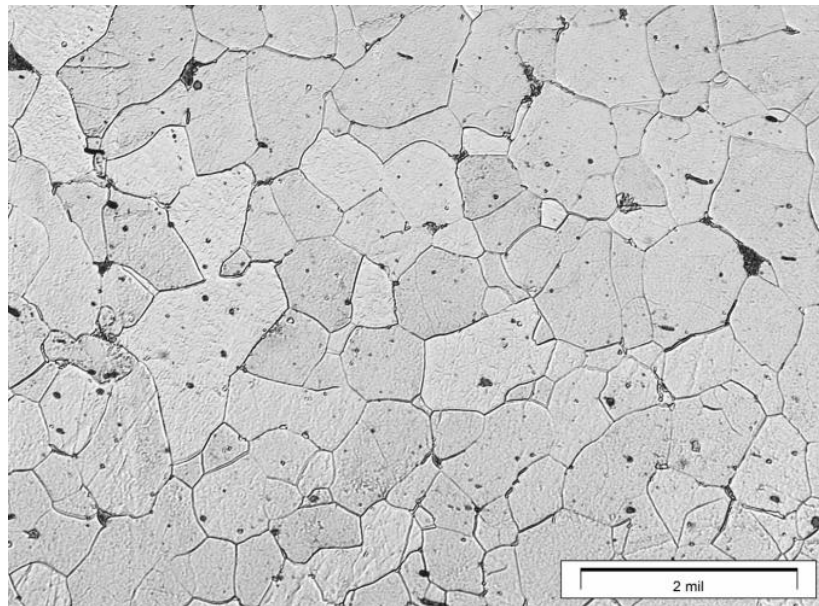
Figure 22. Ferritic microstructure of the failed M174 recoil unit tube material.

2.5 Tubing Design Pressure Proof Load

The failure of hydraulic lines is usually either from a pullout of the tubing or a tubing burst, if the burst pressure is exceeded. In accordance with ASTM-A-254 (*1*), tubing of the size used on the M174 recoil unit should have a proof pressure of ~5.5 ksi. Commercial calculations for the burst pressure of this tubing yield ~10 ksi. A diagram of the likely failure steps for the replenisher/recuperator line can be observed in figure 23.

Step 1

Tube Clamp

Replenisher/
Recuperator
Tube Coupling

Tube Coupling

Operating Tube Configuration

Step 2

Tube Clamp

Replenisher/
Recuperator
Tube Coupling

Tube Coupling

Initial Tube Blow-out

Step 3

1st Tube
Bend

Tube Clamp

Replenisher/
Recuperator
Tube Coupling

Tube Coupling

1st Tube Bending

Step 4

Tube Clamp

2nd Tube
Bend

Replenisher/
Recuperator
Tube Coupling

Tube Coupling

2nd Tube Bending – As-received Tube Configuration

Figure 23. Likely failure steps for the replenisher/recuperator line.

15

The failure of the replenisher/recuperator line on the M174 recoil unit was due to a line pressure event greater than its design pressure. There was no indication that the joint was installed improperly or that there was anything wrong with the materials involved. The ferrule on the failed end was likely flared before installation and was in place only slightly closer to its respective tubing end when compared to the joint on the non-failed end of the tube (via measurements in figures 7–16). Although nonstandard, the joint design was similar to a simple compression joint. This type of joint allows the tubing to slip out of the ferrule and away from its fitting when a given pressure is exceeded. If the joint had been of the flare type, it is likely that the joint would have held, but it might have induced a burst of the line itself, if the maximum burst pressure was exceeded. The cause of the high pressure event remains unknown.
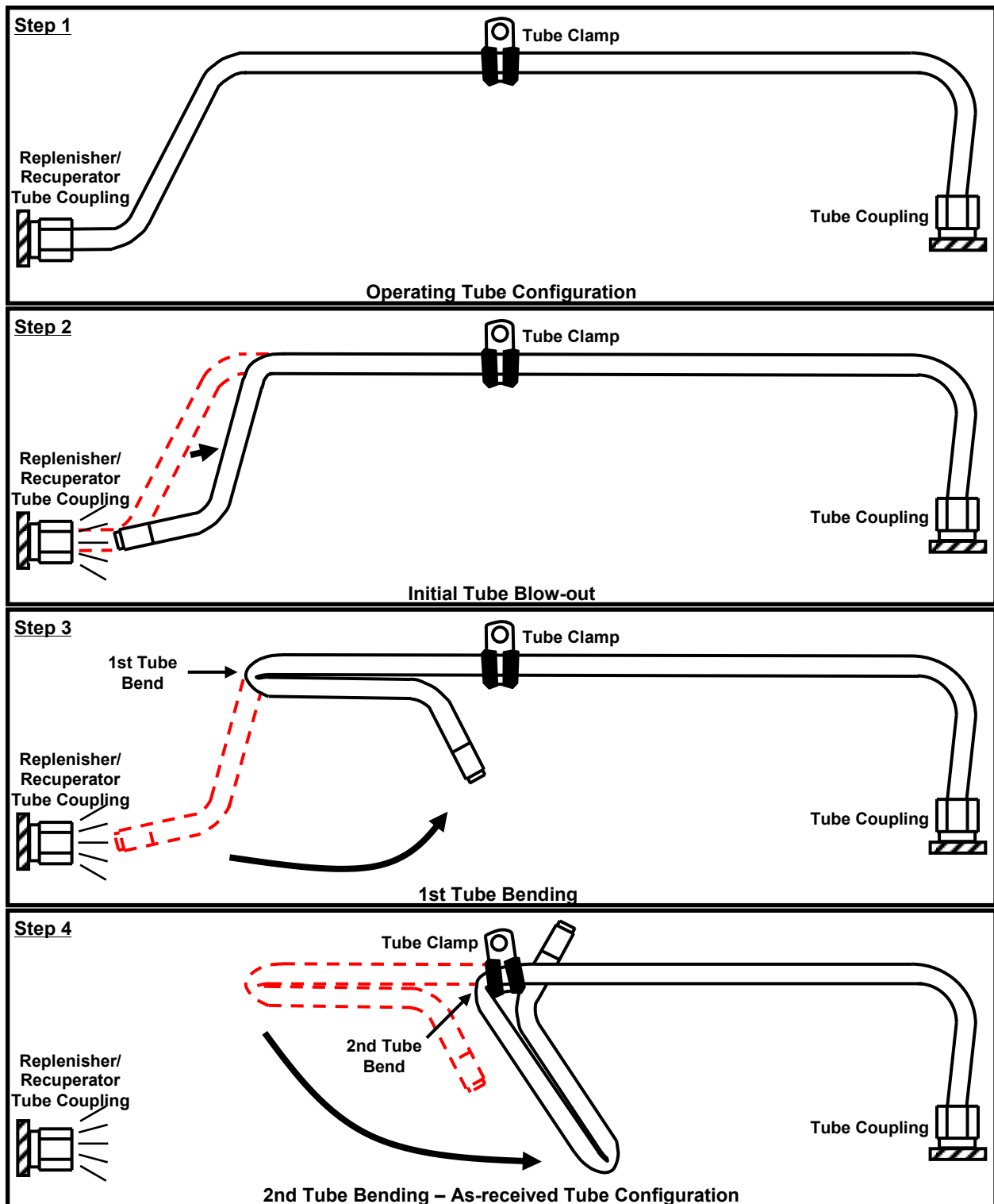
There were two firings related to the October 2010 catastrophic event at EF-9. The first had a calculated chamber pressure of 36 ksi and the second 44 ksi. Since the M11 crusher gauges and measured projectile velocities were in agreement, it is unlikely that a high chamber pressure was the direct cause of the high line pressure within the M174 recoil unit. Two postulates have been forwarded: a time delay in the primary cannon impulse or another internal mechanical failure within the recoil system. After the catastrophic event, the system did not return to the battery position. This may indicate that some other internal recoil mechanism had failed, but it has yet to be confirmed.

3. HARP (M113A1 Cannon) Breech Assembly Spindle

3.1   Visual and Light Optical Examination

The primary focus of the HARP breech failure was on the spindle, although there were secondary fractures to the assembly. The failed spindle can be observed in figure 1 and compared with the geometry of an intact spindle of similar design in figure 24. The mating fracture half from the failed spindle was never recovered. By contrasting the two figures, it can be discerned that the failure of the spindle occurred very near the end of the turned threads on the spindle. Coincidentally, this area is near the exit of the Mk-15 primer cartridge when fitted and locked into the interior bore of the spindle. This relationship can be observed via the simplified schematic in figure 25. From a design perspective, it is likely less than optimum that the exit from the primer charge is located upstream and adjacent to the machined step for the threads. A side-by-side comparison between the failed spindle and an intact example can be viewed in figure 26.

Figure 24. Geometry of an intact spindle, similar to the failed component.
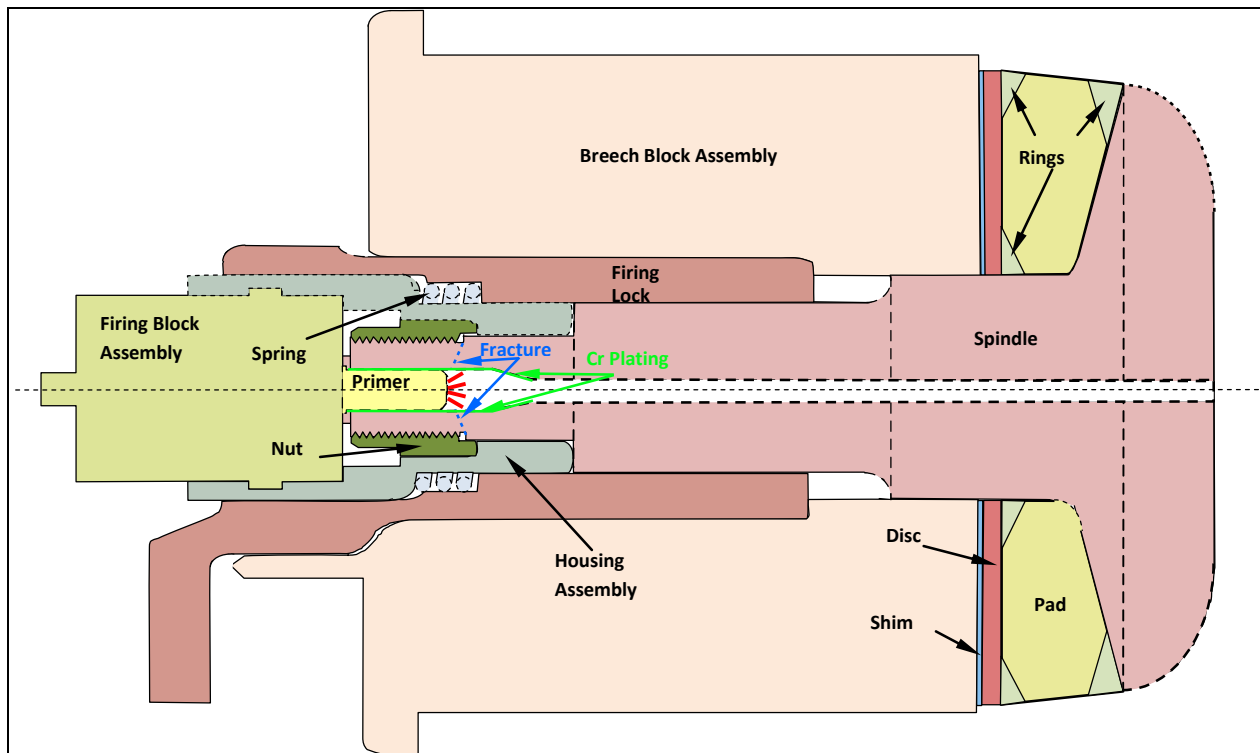
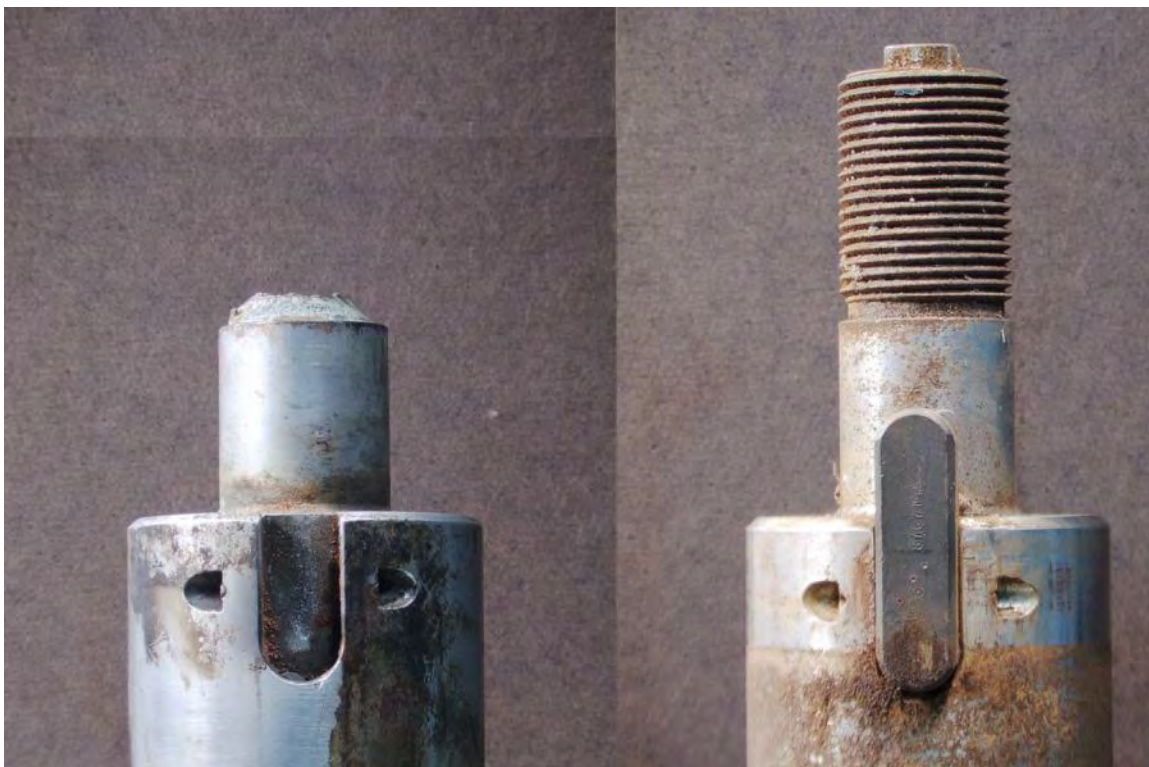Figure 25. Simplified schematic showing the primer/spindle thread proximity.

Figure 26. Side-by-side comparison between the failed and an intact spindle.

The as-received fracture surface can be observed in figure 27. This figure shows some flash rust (orange/brown), residue from primer and/or main propellant wash (blue/green), and three marred metal areas (shiny metallic color) where the fracture was smashed against another hard metal surface. This likely occurred on the second shot during the event against the missing mating fracture half, as this marred surface was well protected inside the recesses of the breech carrier after the catastrophic failure. Greater detail of these marred surfaces and the surface of a circumferential radial crack are presented in figure 28. The figures show considerable hot gas wash over the surface from the primer and main propellant charge. These residues were confirmed through laser induced breakdown spectrometry (LIBS).

Figure 27. As-received spindle fracture surface.

Figure 28. Greater detail of the marred areas and radial crack from the interior.

After the LIBS analysis, the surfaces were delicately cleaned to provide a clearer picture of the
fracture morphology. The cleaned surface is represented in figure 29 and with dimensions
applied in figure 30. After this cleaning, it became obvious that the circumferential radial crack
originated on the interior bore of the spindle. Oblique lighting techniques were applied to
facilitate showing the radial cracks with more detail. Four views of the interior surface taken at
90° rotations are presented in figures 31–34. Enhanced contrast images of these areas are
presented in figures 35–38 to demonstrate the extent of the cracking. This area is normally
covered with chromium plating to prevent this kind of erosion and cracking, as shown in the
schematic of figure 25. However, the enhanced corrosion protection of chromium over steel
does not last forever, and once it is depleted, erosion and cracking of the steel ensues by a
hydrogen-assisted stress corrosion cracking mechanism. The "hydrogen assisted" part of the
mechanism is related to the hot gas propellant wash products forming gaseous hydrogen that is
then absorbed by the steel, embrittling it. There was a great deal of corrosive action evident
from the hot gas propellant wash products on the fracture surface.

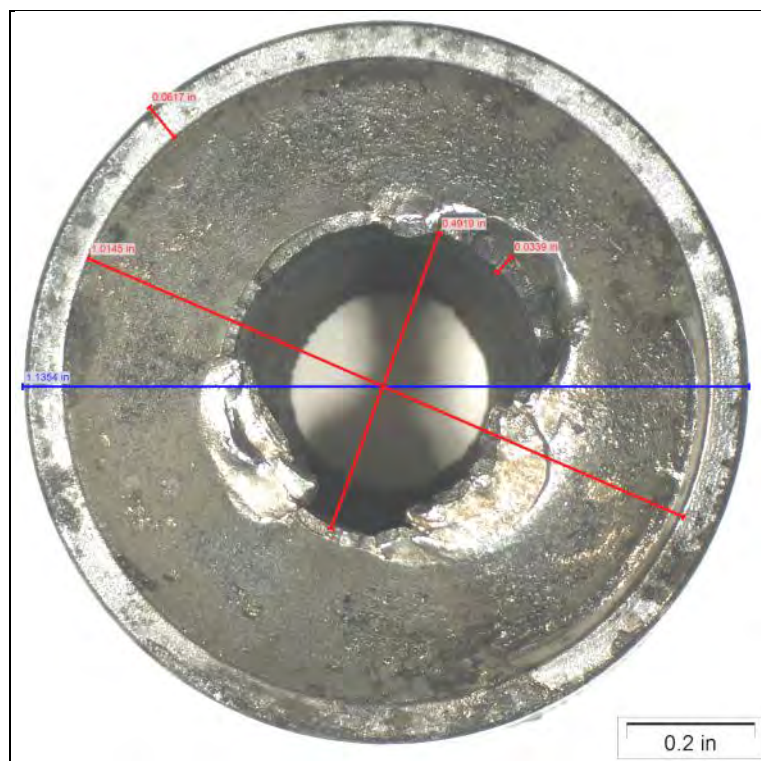Figure 29. Cleaned spindle fracture surface.

Figure 30. Cleaned fracture surface with dimensions.

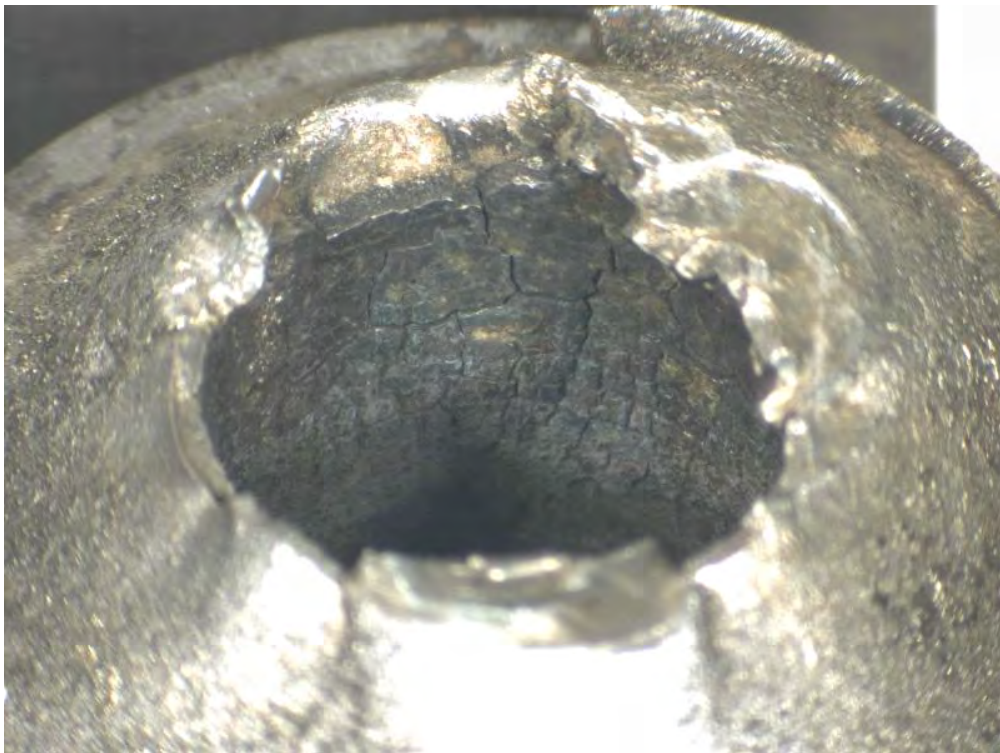Figure 31. Interior bore of the spindle showing cracks.

Figure 32. Interior cracked bore in figure 31 plus a 90° rotation.
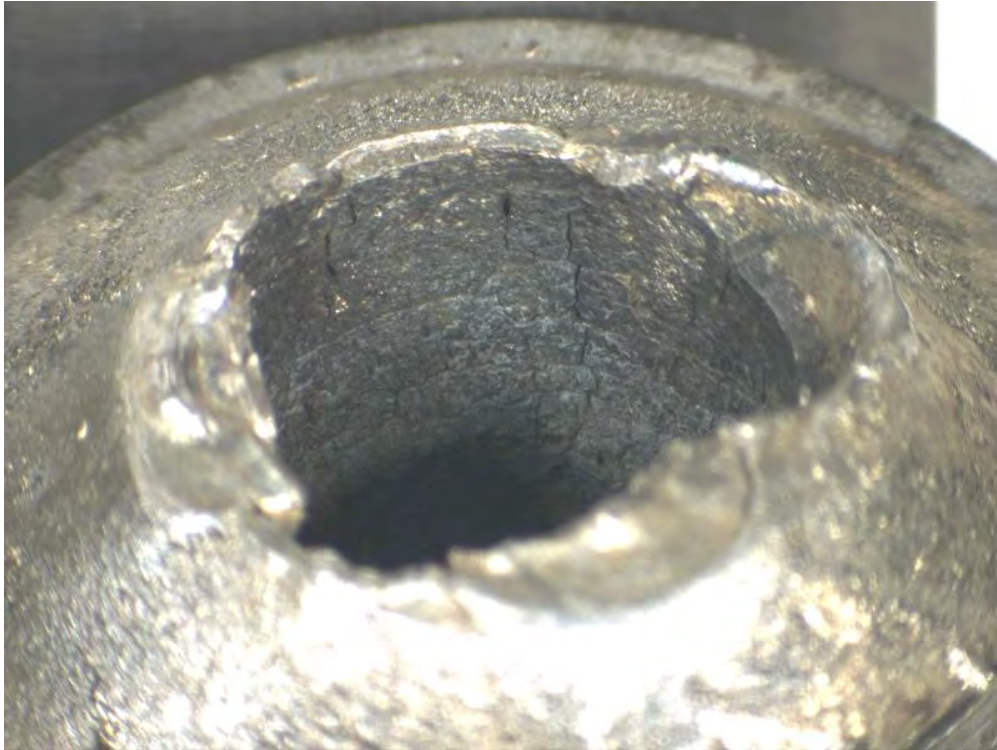
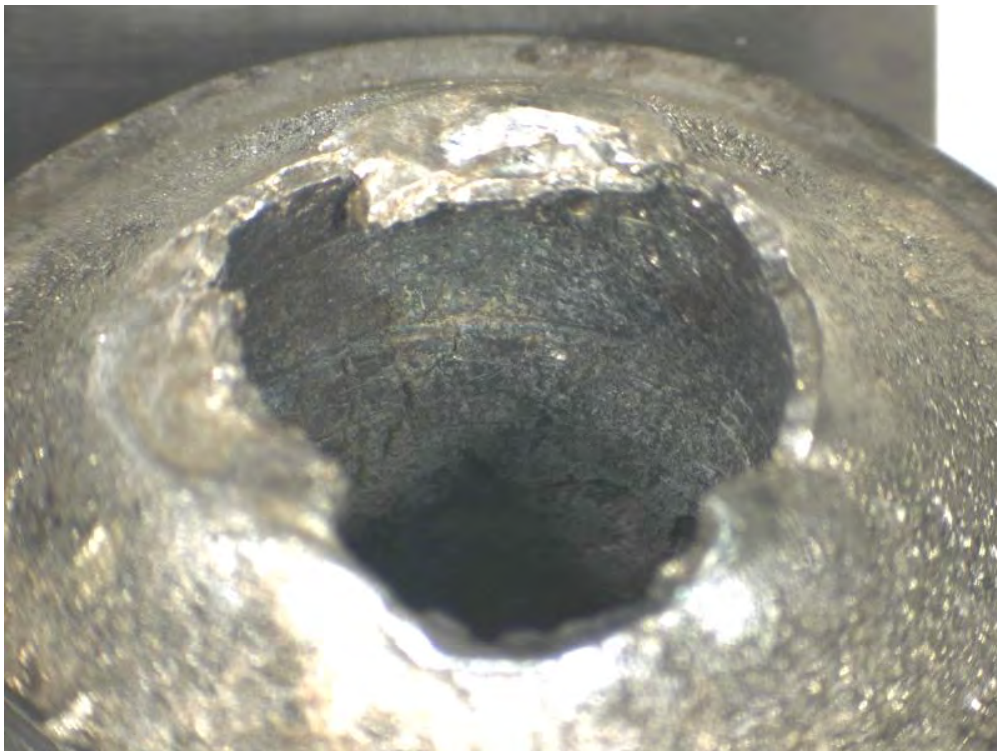Figure 33. Interior cracked bore in figure 32 plus a 90° rotation.

Figure 34. Interior cracked bore in figure 33 plus a 90° rotation.
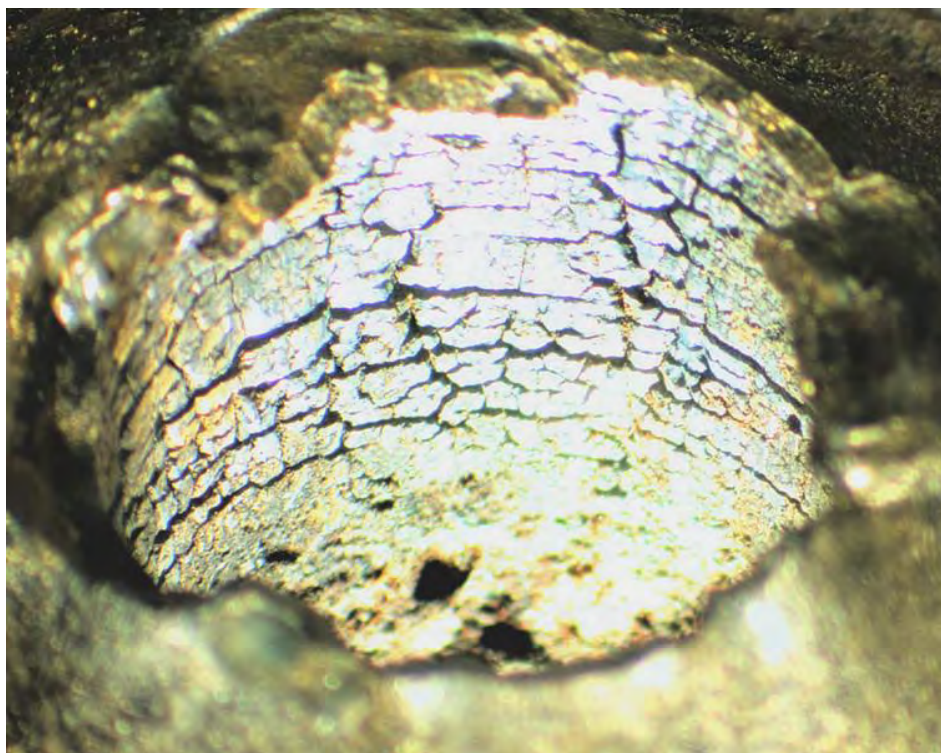
Figure 35. Enhanced contrast image of the area in figure 31.
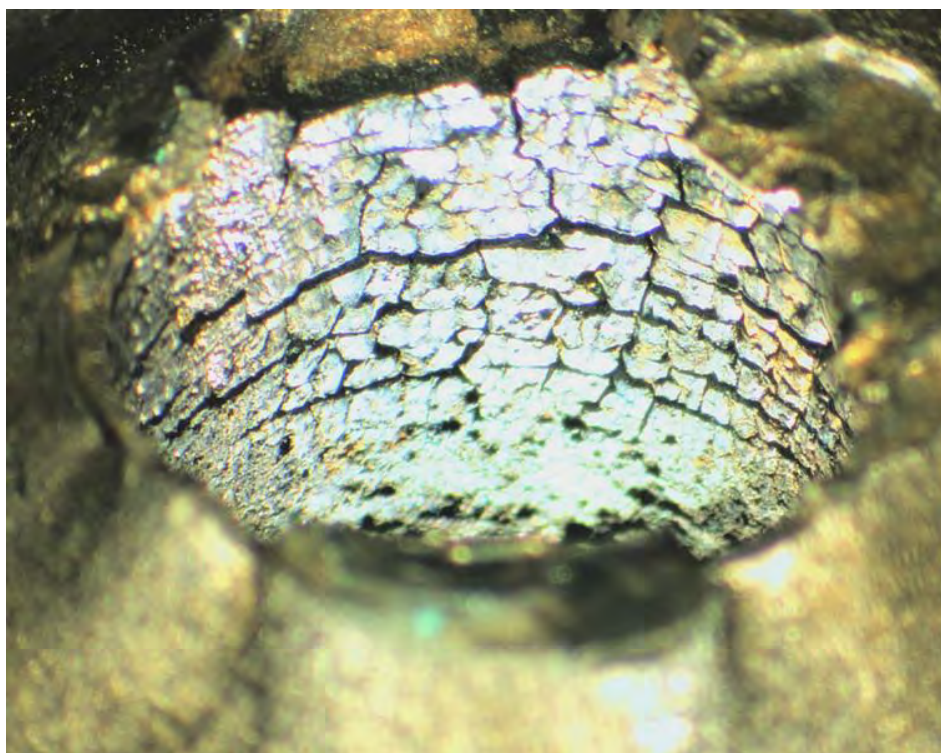

Figure 36. Enhanced contrast image of the area in figure 32.
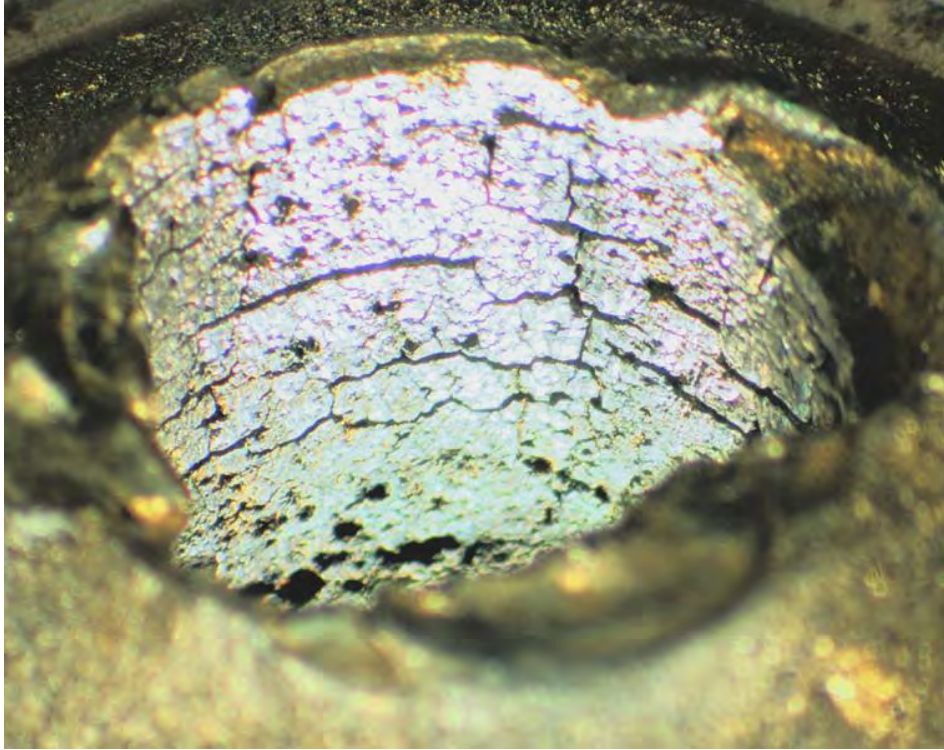
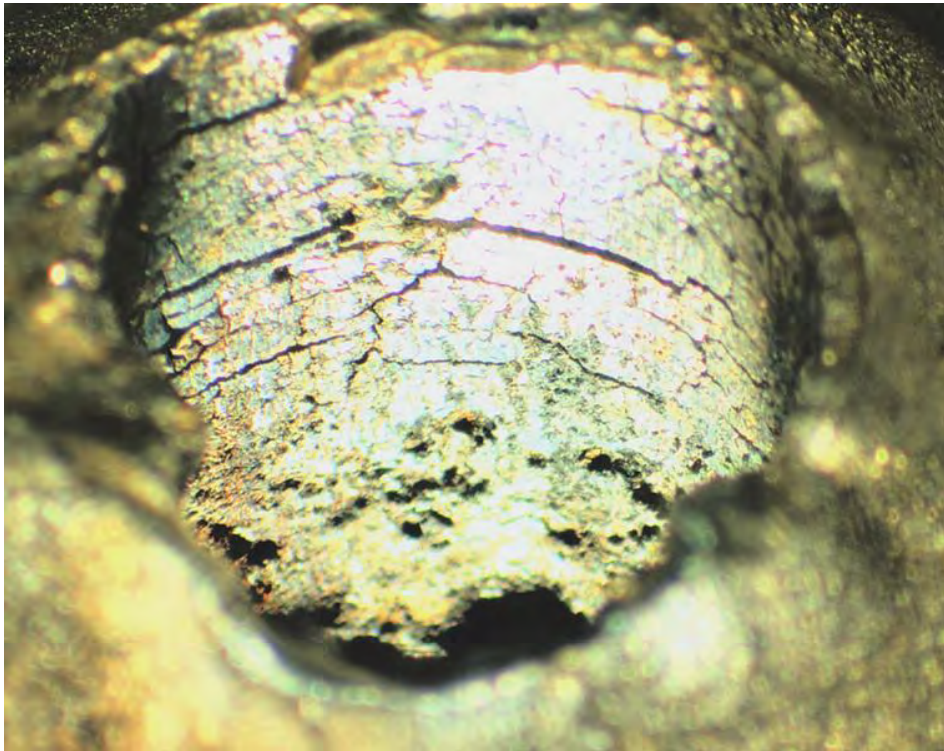Figure 37. Enhanced contrast image of the area in figure 33.

Figure 38. Enhanced contrast image of the area in figure 34.

Oblique lighting techniques were further employed to determine the fracture origin and crack propagation direction. Under this failure mechanism, the cracking would have extended from the interior bore surface and progressed outward radially on several different planes. When the critical flaw size is reached for the loading applied, the material fails when its fracture toughness is exceeded. It is important to note that the fracture toughness is compromised by the absorption of hydrogen. This is discussed in further detail below. The crack origin, in this case, multiple sites, can be observed on the fracture surface presented in the collage of figure 39. The crack directions were determined from the oblique lighting fractography. Although there were three primary origins, there is redundancy shown in the collage. The blue arrows are the crack directions from the primary origins. Red arrows are the crack direction shown after these primary cracks mated up and continued to advance around the spindle. It must be stressed that although there are many arrows, this was a fast event. Metal fracture is generally smoother when slow and rougher when fast. On this surface, the areas where the metal was torn quickly (where the cracks fronts mated) are very rough, and the smoother areas were more slowly separated. The last area to fracture produced a shear lip (the left-hand photograph in the collage of figure 39). The fractography supports that this part failed under two loading cycles. An initial high load cracked it completely (or nearly completely minus the shear lip area). The second loading smashed the fracture surfaces back together, causing the marred areas and then sending the missing fracture half (along with its supporting adjacent components) out the back of the breech assembly. These "high loads" were only high to the hydrogen compromised material. The discussion on fracture toughness below demonstrates that under normal circumstances this component would not have failed.
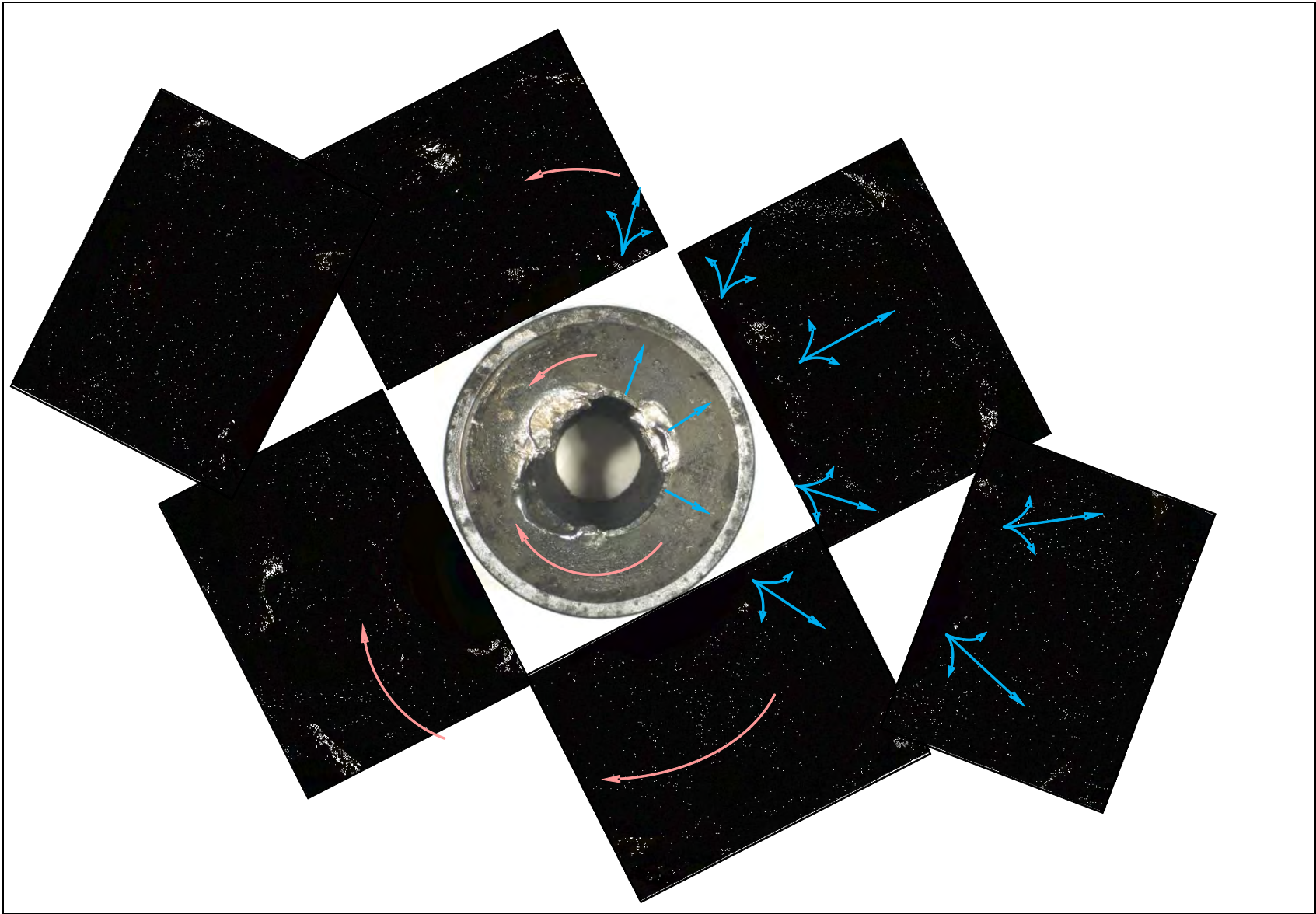
Figure 39. Oblique lighting collage showing fracture origins and crack direction.

A fracture schematic labeling the details discussed previously is presented in figure 40 for clarity and can be compared with figures 27–39. Figure 40 also shows the areas where the scanning electron microscopy (SEM) images were obtained in the next section.
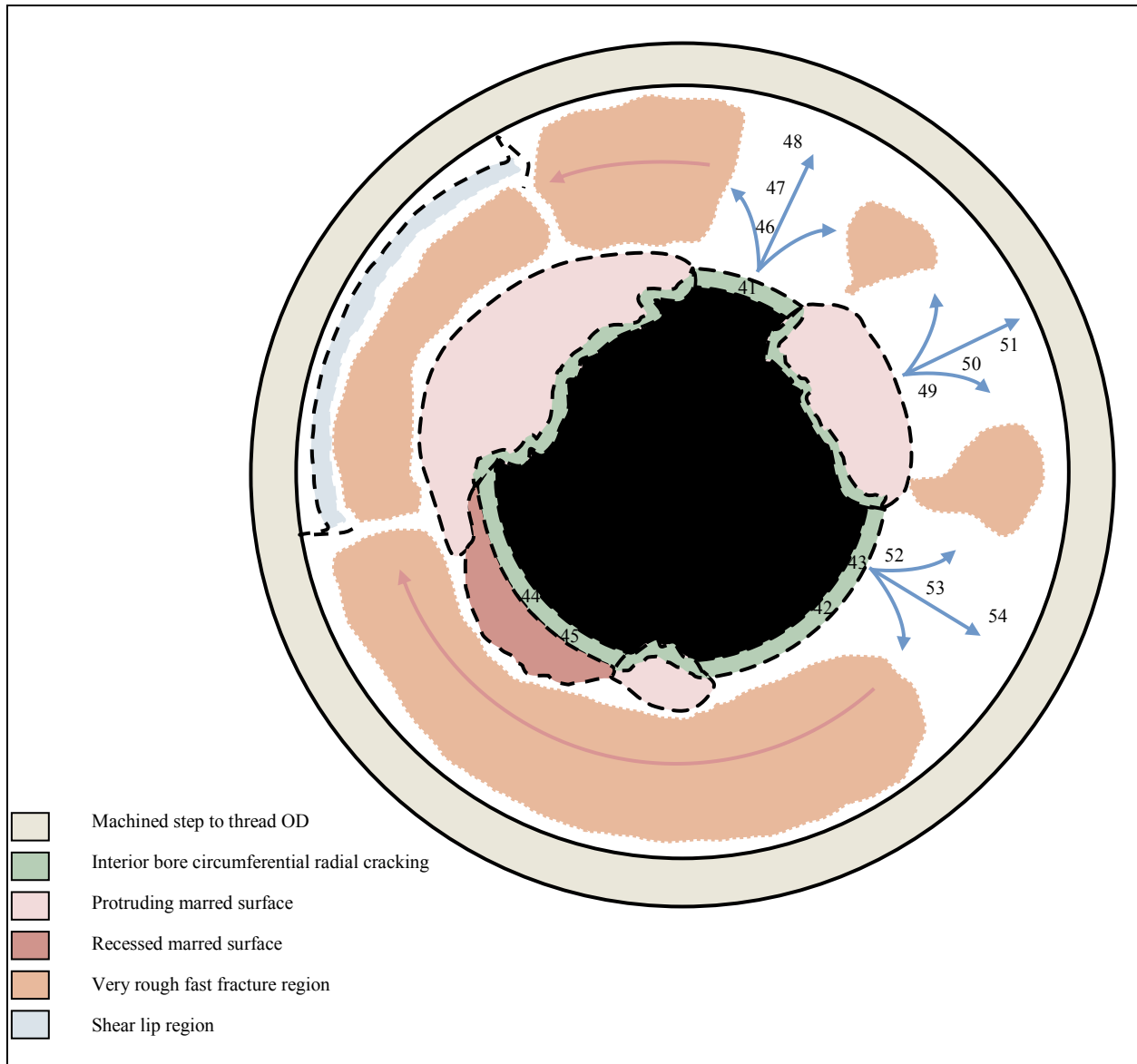

Figure 40. Failed spindle fracture schematic.

3.2   Scanning Electron Microscopy (SEM)

SEM was then conducted on the fracture surface to verify the fracture morphology and confirm the failure mechanism. The surface of the interior bore circumferential radial crack was examined. Figures 41–45 show this surface at various magnifications and demonstrate both the corrosive nature of the mechanism and the intergranular characteristics of the hydrogen effects. The intergranular cracks are denoted with red arrows in the photos.

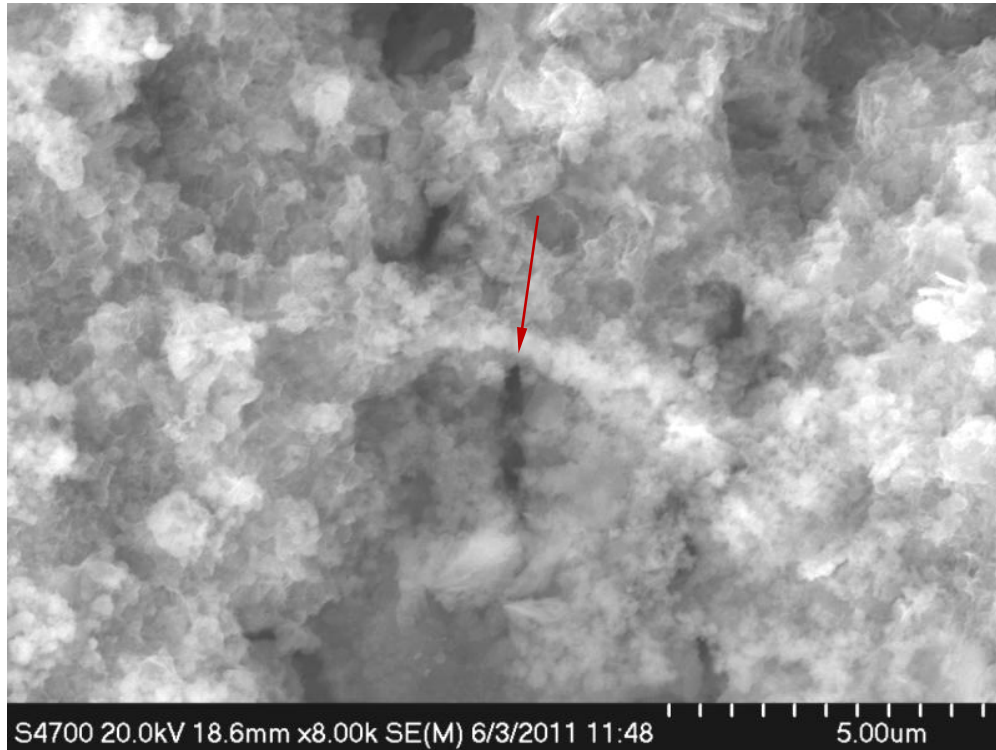Figure 41. Crack from bore showing stress corrosion cracking (SCC) and intergranular cracks, area 41.

Figure 42. Crack from bore showing SCC and intergranular cracks, area 42.
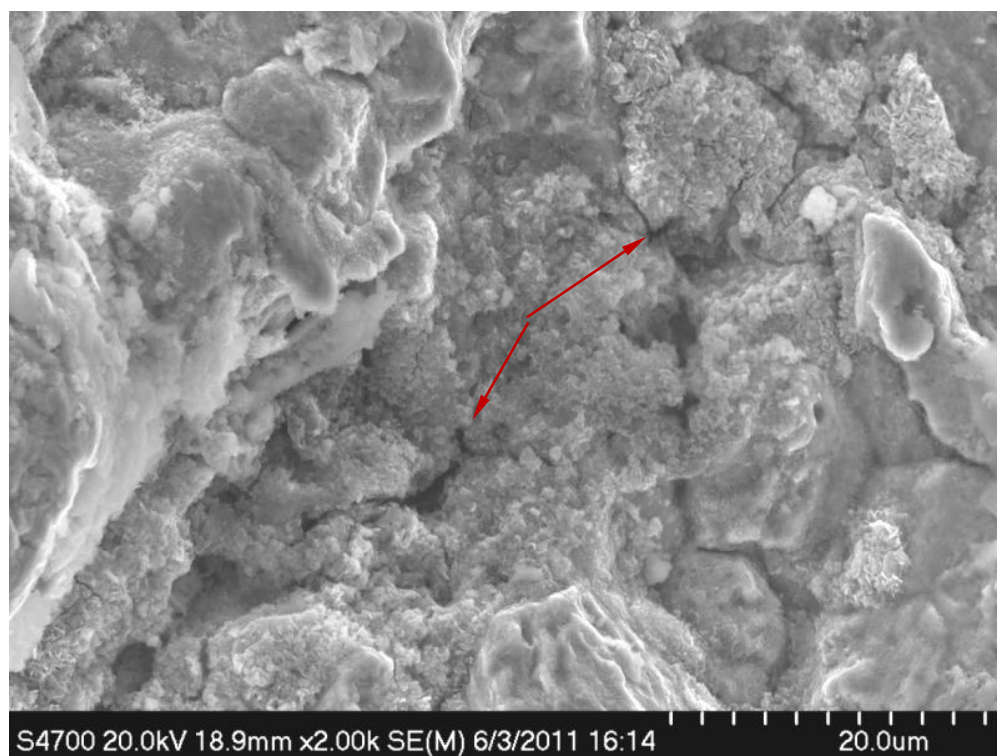
Figure 43. Crack from bore showing SCC and intergranular cracks, area 43.

Figure 44. Crack from bore showing SCC and intergranular cracks, area 44.
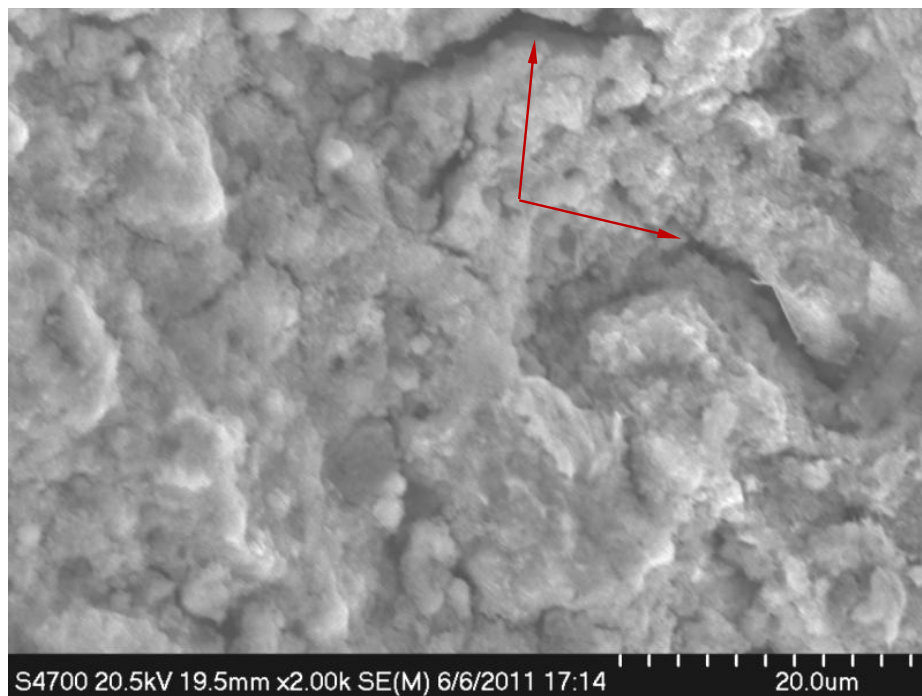
Figure 45. Crack from bore showing SCC and intergranular cracks, area 45.

A linear series of images was then obtained from each of the three fracture origin regions. The minuscule changes in fracture morphology can be observed as the crack progresses in each of the three areas. Figures 46–54 show these three areas, respectively.

Figure 46. Fracture morphology in area 46, as depicted in figure 40.

Figure 47. Fracture morphology in area 47, as depicted in figure 40.

Figure 48. Fracture morphology in area 48, as depicted in figure 40.

33

Figure 49. Fracture morphology in area 49, as depicted in figure 40.

Figure 50. Fracture morphology in area 50, as depicted in figure 40.

Figure 51. Fracture morphology in area 51, as depicted in figure 40.
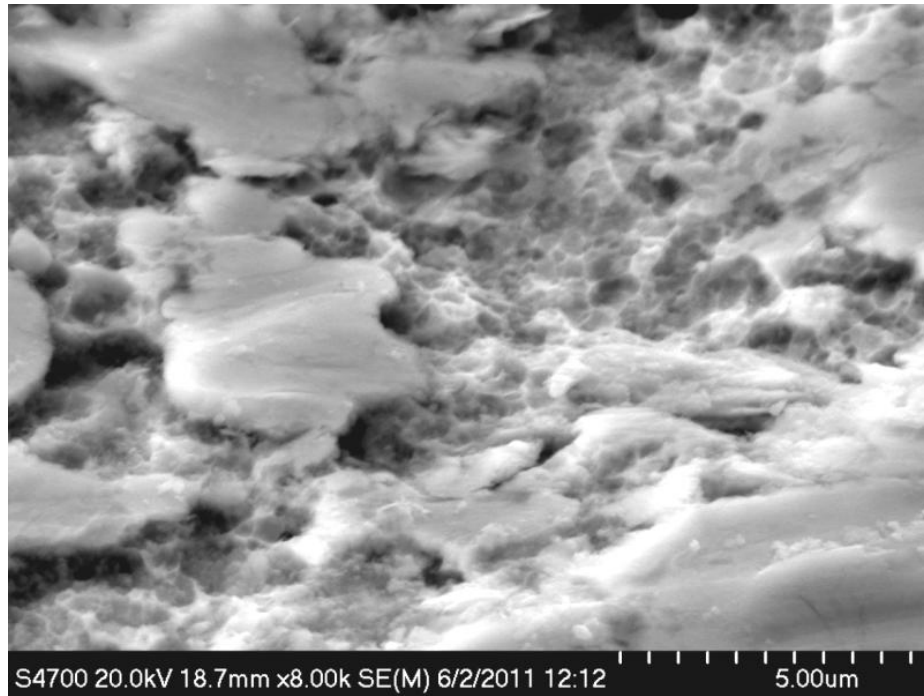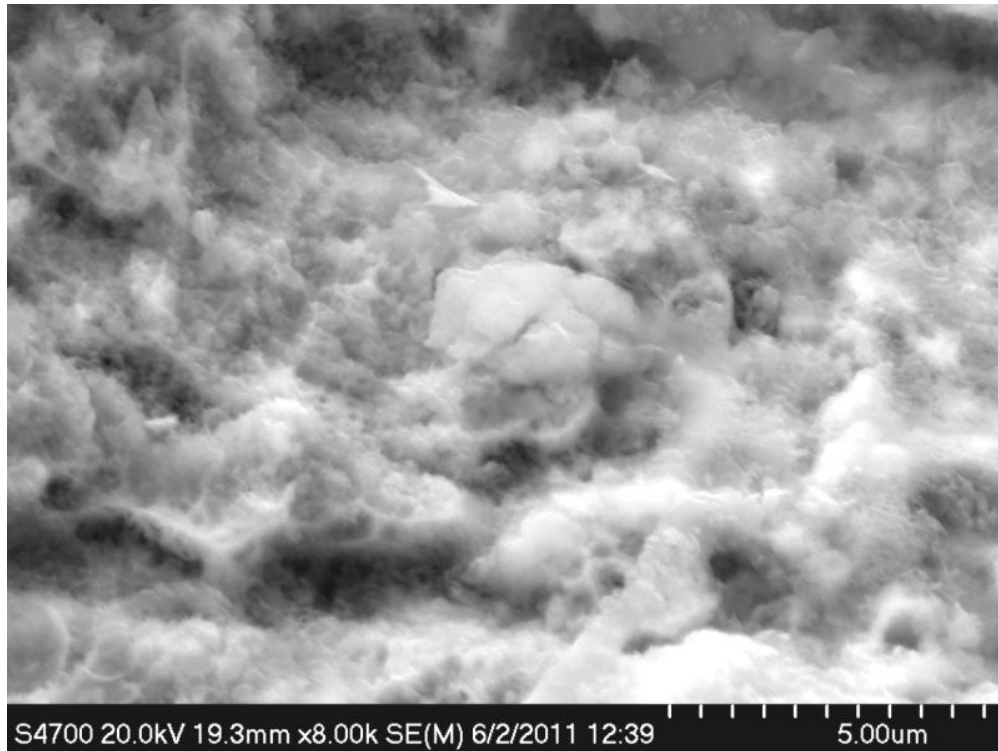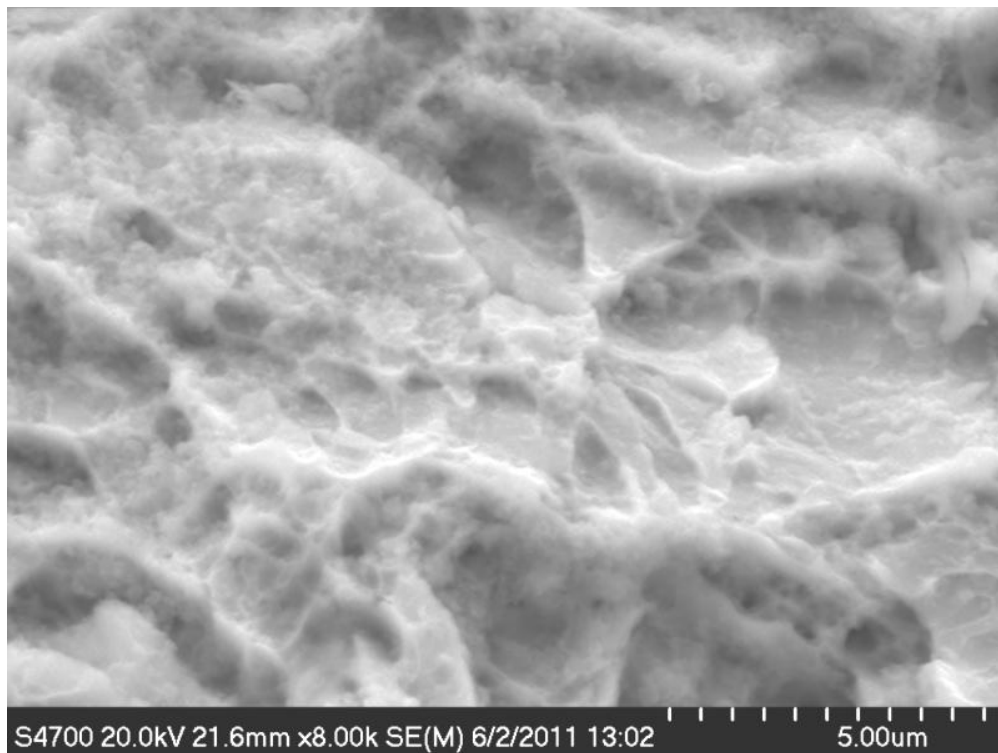

Figure 52. Fracture morphology in area 52, as depicted in figure 40.

Figure 53. Fracture morphology in area 53, as depicted in figure 40.

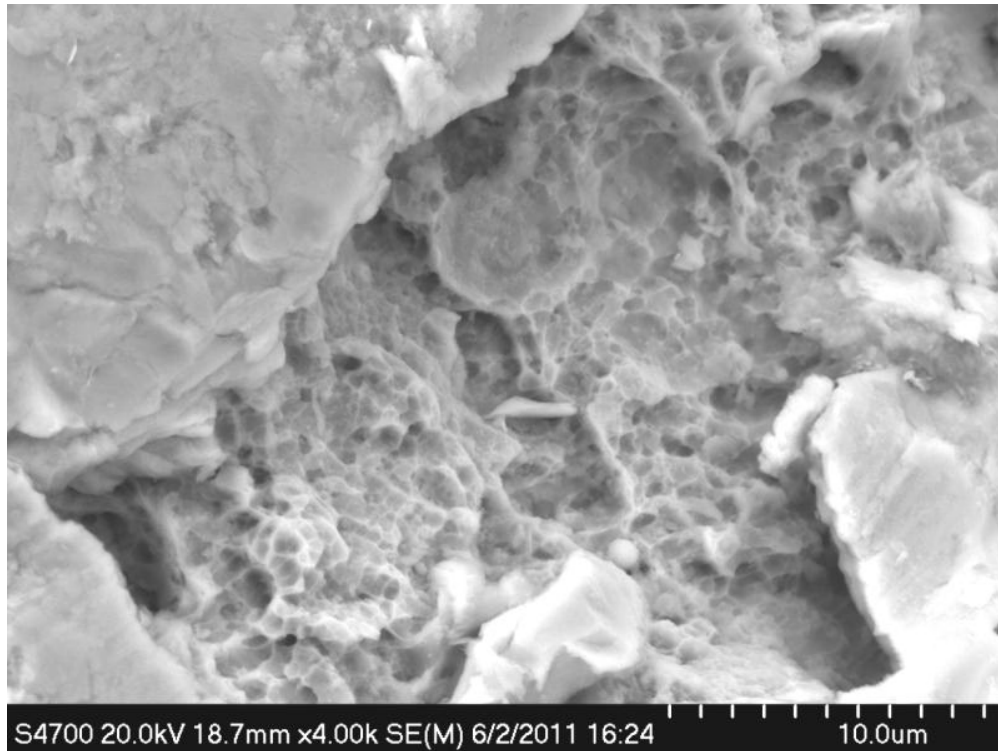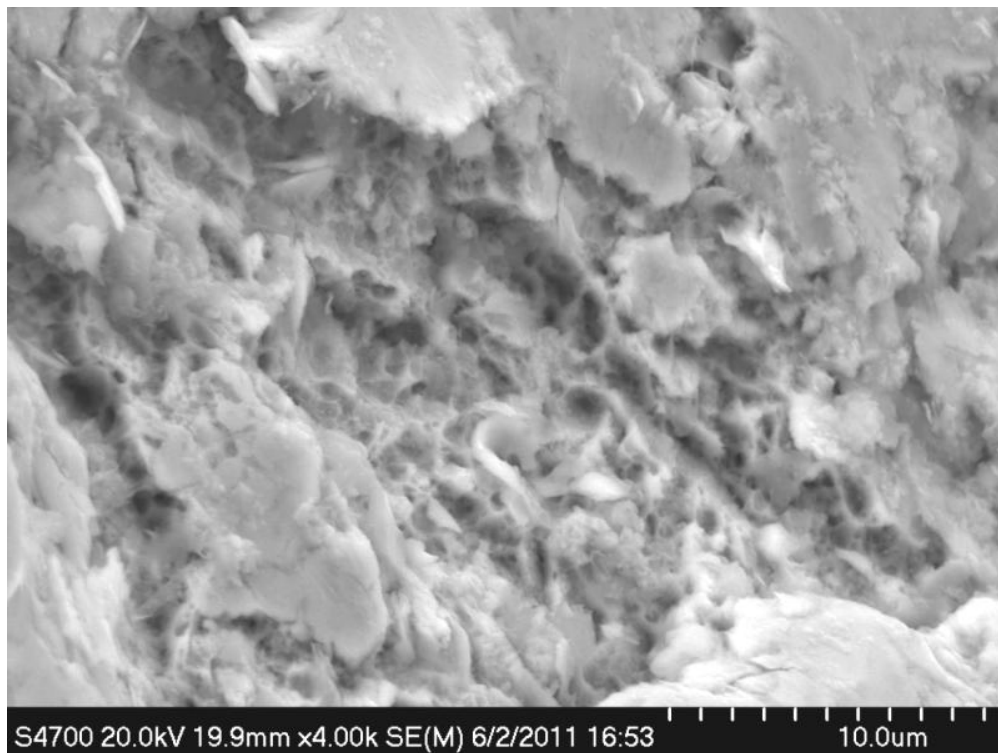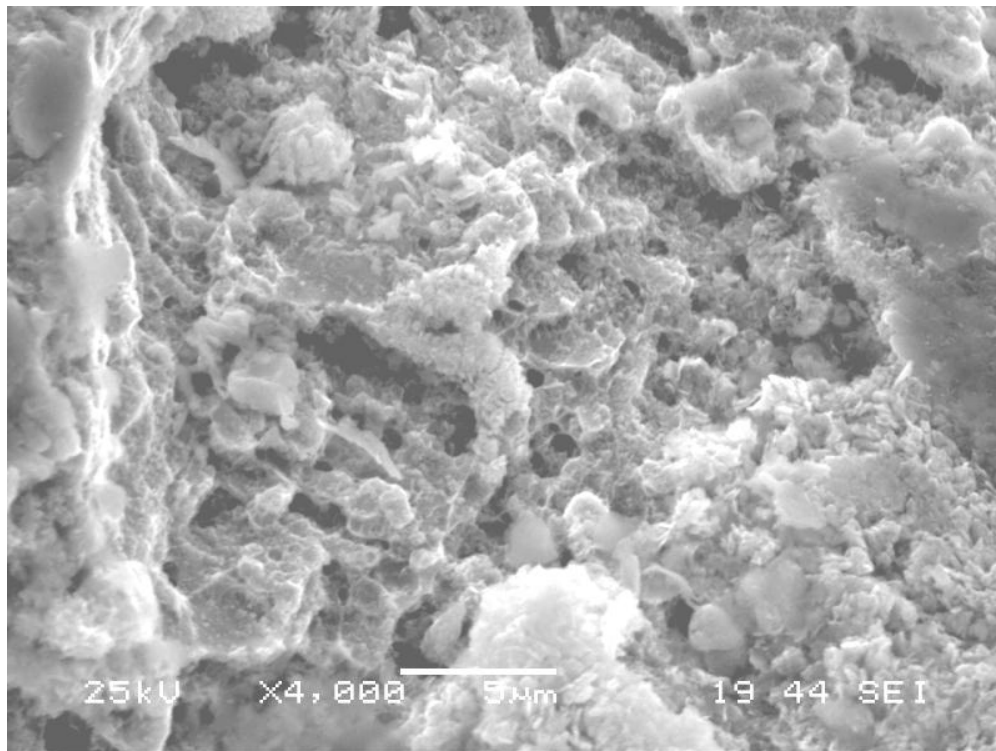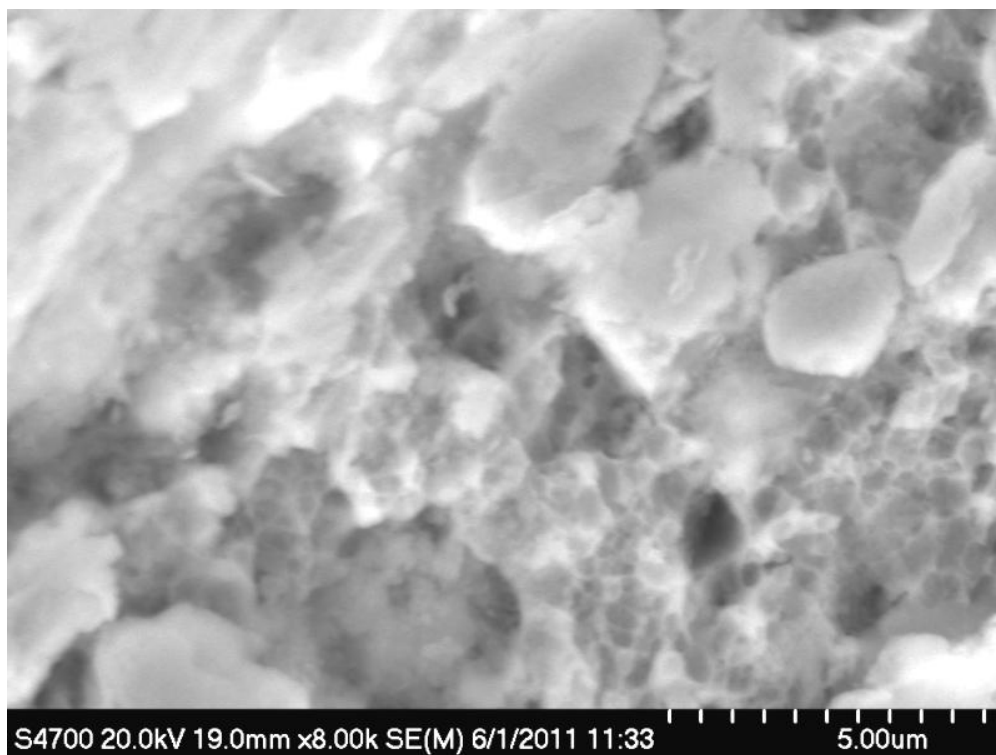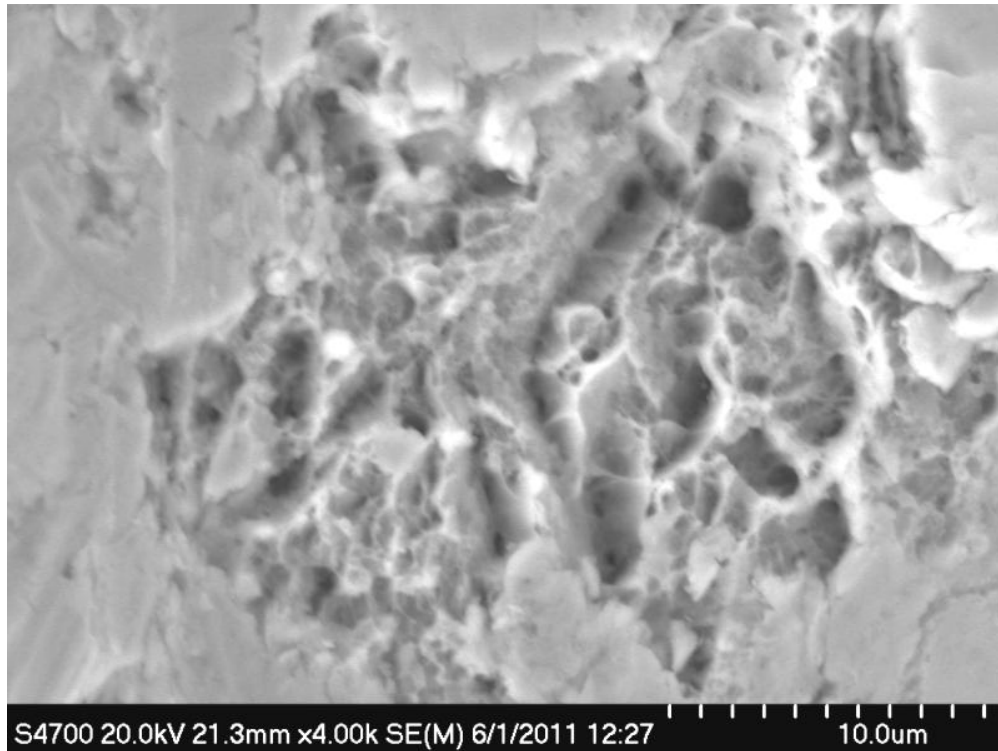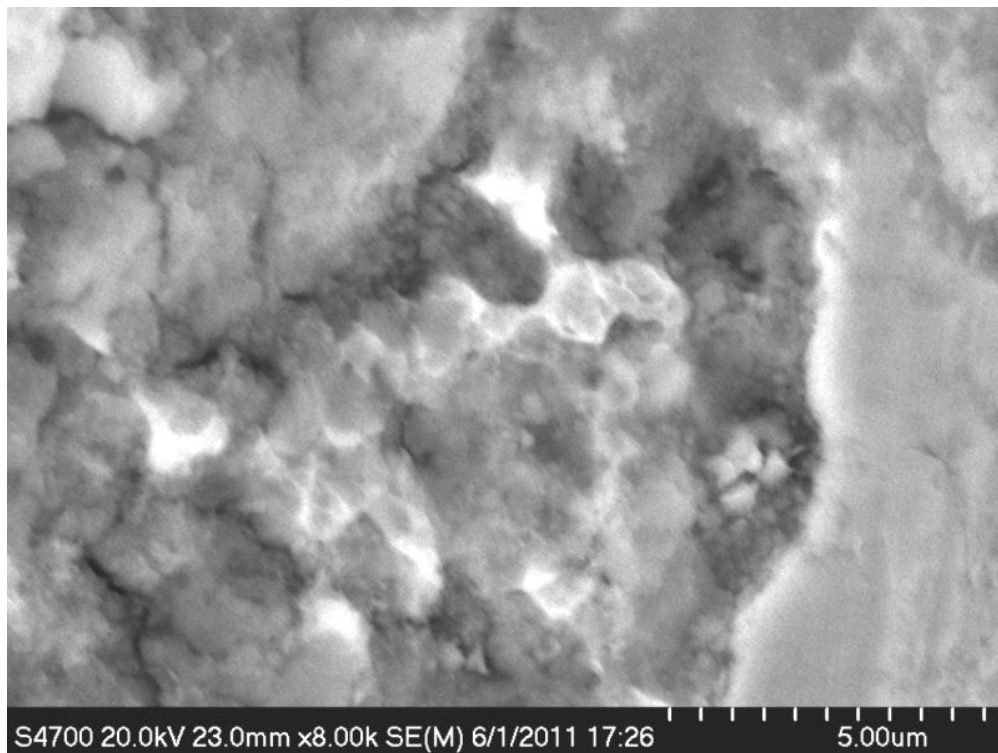Figure 54. Fracture morphology in area 54, as depicted in figure 40.

3.3 Energy Dispersive Spectroscopy (EDS)

EDS was performed to verify the chemical constituency of the 4340 steel alloy. This material was originally procured under MIL-S-5000 (*3*), which has since been cancelled and superseded by SAE-AMS-S-5000 (*4*). The chemical composition conformed to the requirements within the specification. The results of the EDS analysis are presented in figure 55 and in tabular form in table 3. EDS also confirmed that the chromium layer on the interior bore had been eroded away. There were no traces left on the interior surface. The chromium plating was confirmed to exist on the exterior surface in the failed area.
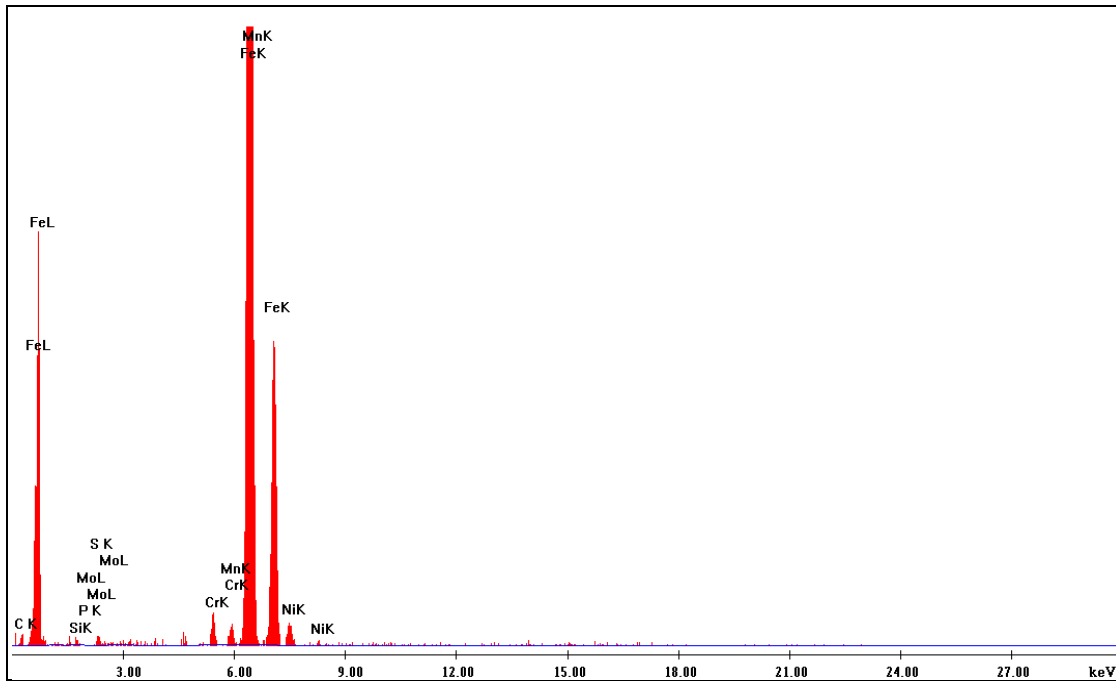
Figure 55. EDS spectrum obtained from the failed spindle material.

Table 3. Chemical composition of the failed spindle vs. accepted values.

Element	Run No. 1 Weight-Percent	Run No. 2 Weight-Percent	Run No. 3 Weight-Percent	Run No. 4 Weight-Percent	Mil-S-5000 (*3*) Values Weight-Percent
Carbon	2.77	2.95	2.82	2.63	0.38–0.43
Silicon	0.26	0.22	0.34	0.27	0.15–0.30
Phosphorus	0.03	0.00	0.00	0.05	0.035 (max)
Sulfur	0.00	0.04	0.03	0.02	0.04 (max)
Chromium	0.66	0.70	0.08	0.03	0.70–0.90
Manganese	0.58	0.84	0.59	0.69	0.60–0.80
Iron	93.78	93.57	93.99	93.89	Balance
Nickel	1.60	1.46	1.48	1.30	1.65–2.0
Molybdenum	0.33	0.22	0.30	0.35	0.20–0.30
Total	**100**	**100**	**100**	**100**	**100**

3.4 Metallography

The microstructure of the spindle was analyzed by polishing and nital etching a cross-sectional mount obtained from a radial cut near the fractured end. Figure 56 shows the cross section revealing the etched microstructure. The structure consists of primarily tempered martensitic lathes and is consistent with that expected for this alloy.
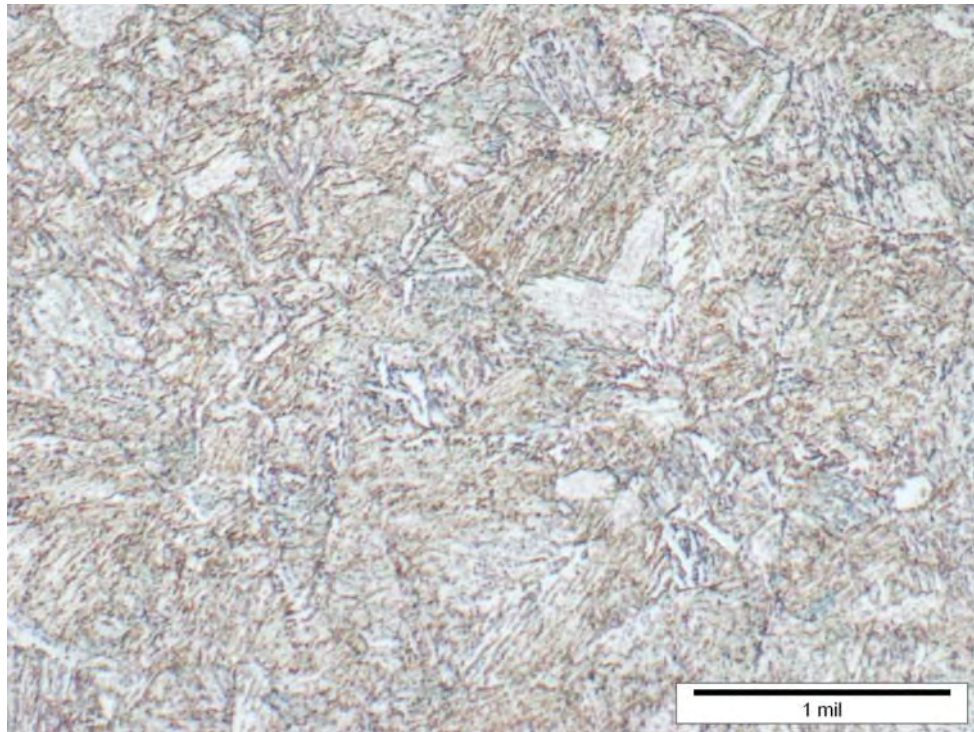
Figure 56. Microstructure of the failed spindle etched with nital.

3.5 Hardness

The hardness of the material was measured with Rockwell Hardness Knoop indentation on a cross-sectional mount in Bakelite. These values were then converted to Rockwell Hardness on the "C" scale, in accordance with ASTM-E-140 (*2*). Table 4 presents the hardness data for the failed spindle. The hardness conformed to that expected from the material, SAE-AMS-S-5000 (*4*) steel.

Table 4. Hardness data for the failed spindle.

Reading Number	Vickers Hardness	Rockwell C Hardness
1	373	34
2	379	35
3	388	36
4	385	35
5	407	37
Average	386.4	35.3
Standard Deviation	12.9	—

3.6   Fracture Toughness

The evidence in the failure of the HARP breech spindle suggests the component failed most likely under a single load cycle. There was a crack-like defect along the circumference of the interior bore in the radial direction. When a component fractures in this manner, the failure is determined by the material property called fracture toughness, or K_{Ic}. The geometry in the failed region is similar to a tube with the radial circumferential crack on the interior wall, as represented by the schematic in figure 57.
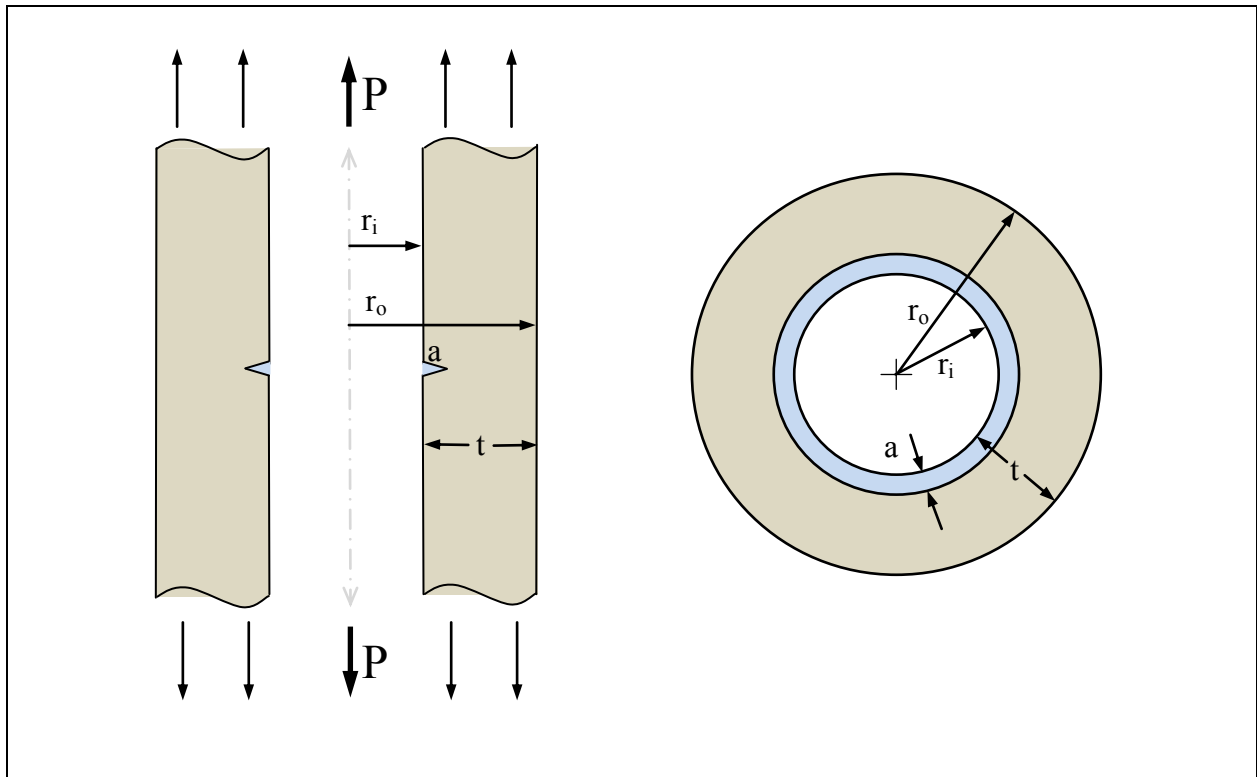
Figure 57. Schematic of the loading on the failed breech spindle.

For this geometry, the fracture toughness is calculated:

$$K_{Ic} = \sigma\sqrt{\pi a} \cdot F\left(\frac{r_i}{r_o}, \frac{a}{t}\right) \tag{1}$$

Tada et al. (5) have calculated numerical solutions for the function, F, as shown in figure 58.

Figure 58. Numerical solutions for the fracture toughness function of a tube.

For the failed spindle case:

a = 0.034 in

t = 0.25 in

r_i = 0.25 in

r_o = 0.50 in

This leaves a/t equal to 0.14 and r_i/r_o equal to 0.50. From the numerical solutions provided, the function value becomes 0.99. If we assume that the breech spindle failed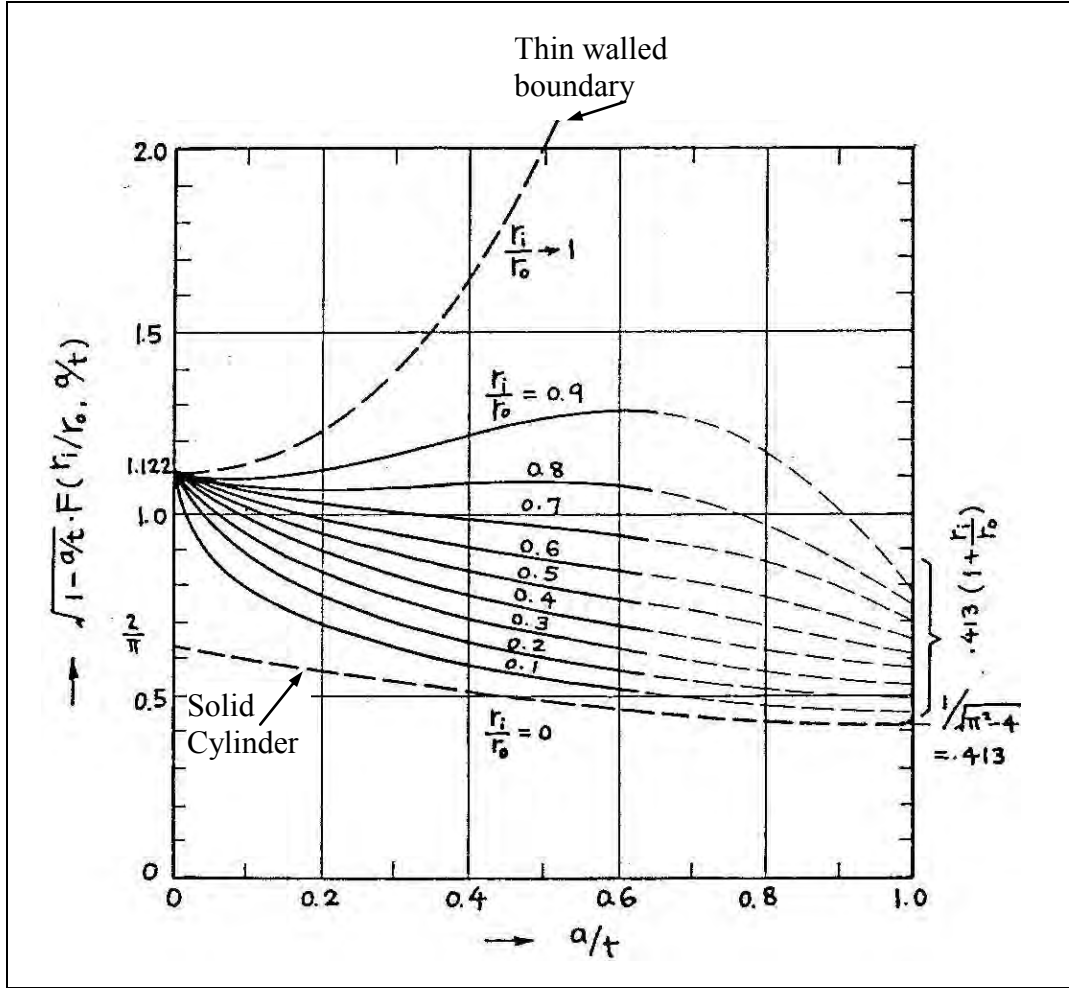 on the first shot during the catastrophic event, as the evidence suggests, the stress on the spindle could be approximated at 36 ksi. The solution for K_{Ic} becomes 11.7 ksi$\sqrt{in}$. The fracture toughness for 35 HRC 4340 steel is nearly 100 ksi$\sqrt{in}$, an apparent conflict. However, in this case, the material was severely hydrogen compromised, as previously discussed. The term K_{Ic} then becomes K_{Iscc}, the SCC fracture toughness. Grendahl (6) has previously shown that the value for K_{Iscc} in (similar, but not identical) HRC 38 vacuum arc re-melted 4340 steel was measured at 13 ksi$\sqrt{in}$, certainly within measureable error for agreement.

4. Conclusions

The following conclusions were drawn from the investigation of the failed components from the HARP catastrophic event at EF-9 in October 2010:

- The failure of the replenisher/recuperator tube on the M174 recoil unit was due to the hydraulic line pressure exceeding the coupling design pressure. Since the main chamber pressure was unlikely to be abnormal, it is thought that some other, yet to be discovered, failure occurred within the interior of the recoil unit.

- The failure of the breech spindle was due to normal loading coupled with a hydrogen compromised material. The influx of hydrogen was made possible by the erosion of the normally protective chromium layer on the interior bore of the spindle. There is no history of anything other than the black powder loaded Mk-15 primer being used in this system. However, the Mk-15 black powder traditionally does not have the adiabatic flame temperature necessary to cause significant erosion of the chromium layer and there is negligible physical erosion in the area. These two facts would suggest that, at some point in the history of this spindle, experimental primers were used, although no evidence of that assertion was uncovered. In any case, the protective chromium layer on the interior bore was worn away and the unprotected steel substrate absorbed hydrogen from the propellant/primer charge byproducts during the normal erosion process while forming cracks on the interior spindle bore. This hydrogen absorption coupled with the cracks lowered the fracture toughness below the critical level for the applied stress on the component. Again, this stress was not abnormally high. Without being hydrogen compromised and without the presence of the interior cracks, this component should have been able to withstand stresses 2.5× higher than that applied during the failure event.

41

5. References

1. ASTM-A-254. Standard Specification for Copper-Brazed Steel Tubing. *Annu. Book ASTM Stand*. 2007 International, West Conshohocken, PA.

2. ASTM-E-140-07. Standard Hardness Conversion Tables for Metals Relationship Among Brinell Hardness, Vickers Hardness, Rockwell Hardness, Superficial Hardness, Knoop Hardness, and Scleroscope Hardness. *Annu. Book ASTM Stand* 2007, ASTM International, West Conshohocken, PA, 2007.

3. MIL-S-5000. *Steel, Chrome-Nickel-Molybdenum (4340) Bars, And Forging Stock* (canceled), 1982.

4. SAE-AMS-S-5000. *Steel, Chrome-Nickel-Molybdenum (E4340) Bars and Reforging Stock*; Society of Automotive Engineers Inc.: Warrendale, PA, 2007.

5. Tada, H. et al. *The Stress Analysis of Cracks Handbook*, Paris Publications Inc., St. Louis, MO, 1985.

6. Grendahl, S. *Environmentally Assisted Cracking Concerns for Cadmium Replacement*; ARL-TR-3099; U.S. Army Research Laboratory: Aberdeen Proving Ground, MD, 2003.

ABERDEEN PROVING GROUND

5   COMMANDER
ABERDEEN TEST CENTER
TEDT-AT-FPM
  R SCHNELL
  J DAMIANO
  E THOMPSON
  T DIETER
  P MARTINELL
BLDG 400
APG MD 21005-5059

1   COMMANDER
ABERDEEN TEST CENTER
TEDT-AT-WFA
  B HARDISKY
BLDG 400
APG MD 21005-5059

3   COMMANDER
ABERDEEN TEST CENTER
TEDT-AT-WFA
  J LAMBERT
  F ROWLAND
  T BUETTNER
BLDG 525
APG MD 21005-5059

25   DIR USARL
RDRL-LOA-T
  J TALSMA
  S CREAMER
  K DUNAWAY
RDRL-LOF
  J ADAMS
RDRL-WML
  M ZOLTOSKI
RDRL-WML-A
  W OBERLE
  F DELUCIA
RDRL-WML-B
  R PESCE-RODRIGUEZ
RDRL-WML-D
  R BEYER
  A BRANT
  J COLBURN
RDRL-WML-E
  P WEINACHT
  B GUIDOS
  J GARNER
RDRL-WML-F
  D LYON
  T BROWN
RDRL-WML-H
  E KENNEDY
  B SORENSON
  R PHILLABAUM
RDRL-WMP
  P BAKER
RDRL WMM F
  S GRENDAHL
  J MONTGOMERY
  M MOTYKA
  B DEROSSET
  S FUDGER
BLDG 4600
APG, MD, 21005-5069